Multi-layered solid-PCM thermocline thermal storage for CSP. Numerical evaluation of its application in a 50MWe plant.

Short title: MLSPCM thermocline numerical evaluation for CSP

P.A. Galione[a,b], C.D. Pérez-Segarra[a,*], I. Rodríguez[a], S. Torras[a], J. Rigola[a]

[a]*Heat and Mass Transfer Technological Center (CTTC),Universitat Politècnica de Catalunya - BarcelonaTech, ETSEIAT, Colom 11, 08222, Terrassa (Barcelona), Spain*
[b]*Instituto de Ingeniería Mecánica y Producción Industrial (IIMPI), Universidad de la República (UdelaR), Uruguay*

Abstract

Thermocline storage concept is considered as a possible solution to reduce the cost of thermal storage in concentrated solar power (CSP) plants. Recently, a multi-layered solid-PCM (MLSPCM) concept —consisting of a thermocline-like tank combining layers of solid and phase change filler materials— has been proposed. This approach was observed to result in lower thermocline degradation throughout charge/discharge cycles, due to the thermal buffering effect of the PCM layers located at both ends of the tank. MLSPCM prototypes designed for a pilot scale plant were numerically tested and compared against other designs of single-tank thermocline systems, such as: solid-filled thermocline, tanks filled with a single encapsulated PCM and cascaded-PCM configurations. Results showed promising results of the MLSPCM configurations for their potential use in CSP plants.

In this work, the MLSPCM concept is used for designing a thermal energy storage (TES) system for a CSP plant with the dimensions and operating conditions of a parabolic trough plant of 50 MWe, similar to Andasol 1 (Granada, Spain). The performance evaluation of each of the proposed prototypes is virtually tested by means of a numerical methodology which considers the heat transfer and fluid dynamics phenomena present in these devices. Two sets of cases are considered, one with the objective of testing the TES systems individually, by defining specific operating conditions and taking the systems to a periodic steady state; and another, aiming to evaluate their performance after several days of operation in a CSP plant, in which the weather variability and the thermal behavior of the tank walls and foundation are simulated. Thermal performance parameters, such as total energy and exergy stored/released and the efficiency in the use of the storage capacity, are calculated and compared with those obtained by other thermocline-like configurations (single-solid and single-PCM), and with a reference 2-tank molten-salt system. Obtained results allow to continue considering the

*Corresponding author
Email addresses: pedrog@cttc.upc.edu, pgalione@fing.edu.uy (P.A. Galione), cttc@cttc.upc.edu (C.D. Pérez-Segarra)

MLSPCM concept as an interesting alternative for thermal storage in CSP facilities.

Keywords: Thermal Energy Storage, CSP, Phase Change Materials, Thermocline, Multi-Layered Solid-PCM, Numerical Analysis

---

NOMENCLATURE

A	Surface area
A_t	Transversal area of tank
A_w	Internal surface area of tank's lateral wall
C_p	Specific heat at constant pressure
d_p	Diameter of filler PCM capsule/solid particle
ex	Exergy
f	Mass liquid fraction (PCM)
F	Capsule volume fraction filled by PCM
g	Gravity acceleration
h	Specific total enthalpy
h_{conv}	Convection coefficient
k	Thermal conductivity
k_{eff}	Effective thermal conductivity
L	Specific latent enthalpy
$m, \dot{m}$	Mass and mass flux
N_r	Number of control volumes of one filler particle/capsule
N_x	Number of tank sections
p	Pressure
$\dot{Q}$	Thermal power
r	Radial direction
R_{cond}	Thermal conduction resistance of capsule shell
R_{conv}	Convection resistance between fluid and capsule/solid filler
t	Time
T	Temperature
U_{TC-Sh}	Heat transfer convection coefficient between the fluid in the packed bed and the tank shell
v	Velocity (seepage velocity in packed beds)
V	Volume
Δt	Time step
Δx	Tank section height
ϵ	Volume liquid fraction (porosity)
η	Efficiency
μ	Dynamic viscosity
ρ	Density

Superscripts and subscripts:

f	Fluid flow
fm	Filler material (PCM or solid)
i	Index of tank section/control volume
$i \pm 1/2$	Index of tank section's face limiting i and $i \pm 1$
in	Tank inlet
j	Index of capsule/solid filler control volume
$j \pm 1/2$	Index of filler control volume's face limiting j and $j \pm 1$
l, liq	Liquid phase
nom	Nominal
out	Tank outlet
s, sol	Solid phase

Abbreviations:

CFL	Courant, Friedrich, Lewy condition
CSP	Concentrated Solar Power
DNI	Direct Normal Irradiation
HTF	Heat Transfer Fluid
MLSPCM	Multi-Layered Solid-PCM
PB	Power Block
PCM	Phase Change Material
SF	Solar Field
TES	Thermal Energy Storage

1. Introduction

Thermal energy storage (TES) allows a more effective use of solar energy by reducing the mismatch between the energy supply and its demand. In concentrated solar power (CSP) facilities, TES systems increase the reliability and generation capacity of the whole system and reduce the levelized cost of electricity [1, 2].

Nowadays, many CSP plants incorporate a molten-salt two-tank TES system (e.g. Andasol and Extresol in Spain, Crescent Dunes and Solana in USA), which makes use of the sensible energy capacity of the molten-salt [3, 4]. However, different TES designs resulting in lower investment costs are currently under study, some of which are also based on the sensible energy capacity of the materials, such as thermocline single-tanks [5, 6] and concrete storage designs [7].

In thermocline systems, both high and low temperature fluids are contained in the same tank. Thermal stratification is the mechanism separating them, and the thermal gradient produced within the fluid is called thermocline. The thermocline thickness indicates the amount of thermal mixing, which may be due to natural convection effects (see e.g. [8, 9]) and strong inlet flow currents [10], and is intended to be maintained at a minimum. A modification to the original concept, aiming at reducing the thermal mixing and also reducing the amount of molten-salt used, is to fill the tank with a cheaper solid material such as quartzite rocks, granite, sand [5], asbestos-containing wastes [11], forming a porous packed bed through which the heat transfer fluid flows.

On the other hand, several researchers have been investigating the use of phase change materials (PCM) as thermal storage media, taking advantage of the high energy density present in the phase-change phenomena. For example, Michels and Pitz-Paal [12] performed a numerical and experimental investigation of storage systems using different PCMs with cascaded melting points, contained in shell and tube heat exchangers, for parabolic trough CSP plants. Liu et al. [13] carried out an extensive review of high-temperature phase change storage materials and of thermal enhancement techniques. Shabgard et al. [14] performed a numerical analysis of cascaded latent heat storage with gravity-assisted heat pipes for CSP applications. Nithyanandam et al. [15] studied packed bed thermal storage with encapsulated PCMs for CSP by means of a numerical model. They performed parametric analyses and established guidelines for the design of latent storage systems. Flueckiger et al. [16] analyzed latent-heat-augmented thermocline storage for CSP using an integrated system-level model for the whole CSP plant and evaluated the effect of the increase of the storage capacity with the latent heat. Limitations in the thermal performance of tanks including PCMs were observed, while some improvement was obtained with some of the cascaded PCM designs.

Furthermore, Steinmann and Tamme [17] studied the combination of latent and sensible storage heat exchangers specially suited for direct steam generation solar field technology (DSG). A PCM storage unit was intended for producing the vapor generation (evaporation) and two concrete storage units for storing the sensible portion of the fluid's energy (pre and superheating).

In previous works [18, 19], a new concept of thermocline-like thermal storage device named multi-layered solid-PCM (MLSPCM), consisting of a packed bed of different layers of solid and PCM filler materials, was presented. There, MLSPCM designs of the same dimensions and operating conditions as those of the pilot scale tank presented by Pacheco et al. [5], were numerically tested and compared against other designs of single-tank thermocline-like systems such as: single-solid, single-PCM and cascaded-PCM filler configurations. Results obtained for MLSPCM prototypes showed to be promising for their potential use in CSP plants.

In this work, the MLSPCM concept is used for making up a TES system for a CSP plant. A parabolic trough of 50MW of electric output is assumed, similar to Andasol 1 plant (Granada, Spain). With this aim, two levels of analysis are carried out. Firstly, numerical simulations similar to those presented in [18] are carried out, in order to evaluate the performance of the full-scale TES prototypes under specific conditions. In these, the TES is charged and discharged consecutively until reaching a periodic steady state. Secondly, in order to test the different TES systems under operating conditions closer to those of a CSP facility, another analysis is performed incorporating weather variation, idle processes and thermal losses to the tank shell and foundation, for several days of plant operation. For this, a modular object-oriented code is used [20], which links the different models corresponding to the elements under study.

Similarly as in the pilot-scale prototypes presented in [18, 19], some full-scale MLSPCM configurations are observed to produce an increase of the efficiency in the use of total capacity when compared with other thermocline-like designs, especially in the isolated TES analysis. Although consideration of the variability of the operating conditions results in closer values of accumulated energy and efficiency, MLSPCM concept continues to present advantages over the solid-filled thermocline design. The advantages against single-PCM packed beds are more clear, since a similar storage is obtained using a much lower amount of encapsulated PCM, which is assumed to be a costly component compared to the solid filler material. As a result of the study, a MLSPCM prototype considered equivalent to the reference 2-tank system is presented, resulting in the same amounts of energy and exergy delivered to the power block in both analyses.

1.1. MLSPCM concept

Figure 1 shows a sketch of a three-layered MLSPCM TES tank. It consists of a tank containing a porous bed through which a fluid passes delivering/absorbing energy to/from the filler material, as in a “conventional” thermocline tank. However, the MLSPCM concept uses a combination of layers of different filler materials, with one solid and at least one containing PCM. The PCM layers are placed in the extremes of the tank, and their melting points are chosen to be within the admissible temperature ranges for the fluid coming out of the tank through the outlet located close to the PCM filler. These ranges are determined by the HTF temperature required by the solar receivers (in the TES charging process) and the power block (in the TES discharge), which impose temperature thresholds to HTF inflow, for their proper operation.

In a MLSPCM with three layers, as that shown in Figure 1, the PCM located at the top is chosen to have a high melting point (within the admissible range of temperatures for the fluid coming out in the discharge process), and the one located at the bottom is chosen with a low melting point (within the range admitted for the outflow in the charge process).

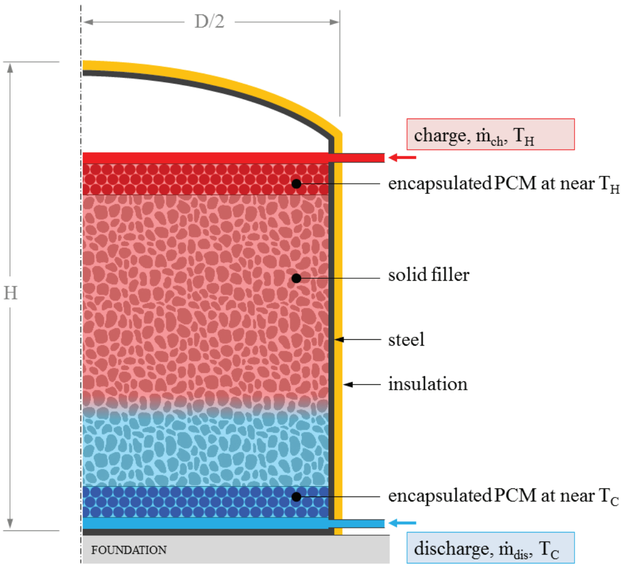

Figure 1: Sketch of a MLSPCM TES tank with three layers

The PCM layers not only increase the total storage capacity of the TES tank (with respect to a single-solid filled tank), but also act as thermal "buffers" by keeping the outflow temperatures within the admissible temperature ranges. Therefore, there is an increase in the operating time (since the processes can continue while the outflow temperatures remain within these ranges), and thus in the amount of energy which can be effectively stored/withdrawn, resulting in a high efficiency in the use of the total (ideal) storage capacity.

2. Mathematical modeling and numerical implementation

The thermocline-like TES considered are formed by different elements: thermocline packed bed (filler material and HTF), tank foundation and tank walls, which interact with each other through their boundary conditions. This implementation has been performed within the NEST platform [20], which allows linking between different elements of the thermal system. The mathematical model considers the transient behavior of the thermocline-like packed beds, the tank walls and insulation, taking into account the variable outdoor conditions (DNI, ambient temperature). A brief mathematical description, focused on the modeling of the packed bed, is presented hereafter.

2.1. Packed bed

The model presented in [18] is used. Mass, momentum and energy conservation equations have to be solved in order to be able to simulate the thermal behavior of a thermocline-like tank. One-dimensionality in the fluid flow and in the heat transfer inside particles/capsules is assumed. Natural

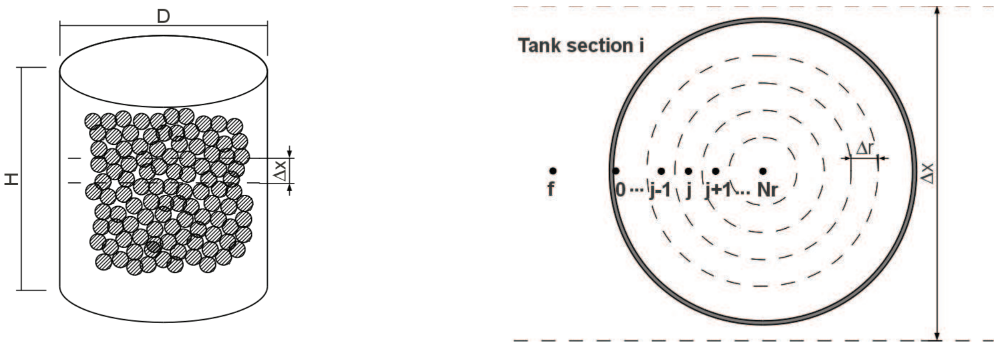

(a) Sketch representing the cylindrical container with the PCM capsules packed in a random fashion

(b) discretization details of the tank and of a representative particle/capsule, indicating the sub-indices used for tank sections (i) and capsule control volumes (j)

Figure 2: Domain and discretization.

convection and contact melting inside PCM capsules is neglected, as well as thermal conduction between different particles/capsules.

In the filler particles/capsules, a radial variation of the temperature is assumed. Conservation equations are discretized using the Finite Volume Method (FVM). The tank is divided in N_x transversal cylindrical sections of height Δx (see Fig. 2a). In each tank section, a single representative particle/capsule needs to be simulated, due to the one-dimensionality assumption. This filler particle/capsule is discretized in the radial direction in N_r control volumes, as shown in Fig. 2b.

For the heat transfer fluid (HTF) going through the porous bed, the semi-discrete energy conservation equation of the fluid in the i$^{\text{th}}$ tank section ($i = 1...N_x$) results in:

$$\begin{aligned}\rho_f \epsilon_i V_i C_{p,f} \frac{\partial T_{i,f}}{\partial t} &= A_t \left(k_{eff} \frac{\partial T_f}{\partial x} \right) \Bigg|_{i-1/2}^{i+1/2} - \dot{m} C_{p,f} (T_{i+1/2,f} - T_{i-1/2,f}) \\ &- n_{fm,i} \frac{T_{i,f} - T_{i,0}}{R_{conv,i} + R_{cond,i}} - U_{TC-Sh} A_{w,i} (T_{i,f} - T_{i,Sh})\end{aligned} \tag{1}$$

where $T_{i,0}$ is the temperature of the internal surface of the particles/capsules (boundary node in fig. 2b). In the advective term (second in the right hand side) the fluid is assumed to be coming from section $i-1$ and going to section $i+1$.

R_{cond} stands for the thermal resistance in the PCM capsules due to the capsule shell. The mass of the shell is disregarded here and is not considered to add any thermal inertia. The calculation of the thermal resistance due to convection between the HTF and the filler material (R_{conv}) requires the fluid-to-bed Nusselt number, which is calculated using the correlation obtained from [21]:

The effective thermal conductivity (accounting for solid-phase conduction and thermal dispersion) is evaluated as the sum of stagnant and dispersion effective conductivities, calculated with the correlations obtained from [22] and [23].

The energy balance for the inner nodes ($j = 1...N_r$) of the filler material (either PCM capsules or solid particles) remains:

$$\rho_{fm} F_i V_{i,j} \frac{\partial h_{i,j}}{\partial t} = \left(k_{fm} A \frac{\partial T}{\partial r} \right)_{i,j-1/2} - \left(k_{fm} A \frac{\partial T}{\partial r} \right)_{i,j+1/2} \tag{2a}$$

while for the boundary node ($j = 0$), in contact with the heat transfer fluid, results in:

$$\rho_{fm} F_i V_{i,0} \frac{\partial h_{i,0}}{\partial t} = \frac{T_{f,i} - T_{i,0}}{R_{conv,i} + R_{cond,i}} - \left(k_{fm} A \frac{\partial T}{\partial r} \right)_{i,1/2} \tag{2b}$$

where F_i indicates the volume fraction of the capsules occupied by the PCM (F_i=1 for the solid particles). This value is between 0 and 1 and takes into account that a void space is needed in order to allow for the thermal expansion in the melting.

The relations between enthalpy and temperature for the filler materials (solid and/or PCM) are:

$$\begin{aligned}
h - h_0 &= C_{p,s}(T - T_0), && T \leq T_s \\
h - h_0 &= C_{p,s}(T - T_0) + fL, && T_s < T \leq T_{sl} \\
h - h_0 &= C_{p,l}(T - T_{sl}) + C_{p,s}(T_{sl} - T_0) + fL, && T_{sl} < T \leq T_l \\
h - h_0 &= C_{p,l}(T - T_{sl}) + C_{p,s}(T_{sl} - T_0) + L, && T_l < T
\end{aligned}$$

where T_{sl} indicates the temperature in the phase change range chosen as the transition temperature for the specific energy from solid to liquid, or vice versa. Mass liquid fraction (f) ranges from 0 (pure solid) to 1 (pure liquid) and is calculated as a linear function of temperature in the phase change interval:

$$f = \frac{T - T_s}{T_l - T_s} \tag{3}$$

By taking a very narrow temperature range ($T_l - T_s$), fixed melting point PCMs can also be modeled with this approach. Hence, a unique value of h exists for each value of T, and the energy balance (Eq. (2)) is expressed with T as the only variable.

For evaluating the power generating potential of the energy delivered by the thermal storage, the exergy global balance of the heat transfer fluid is calculated in the following manner:

$$\dot{m}(ex_{out} - ex_{in}) = \dot{m} C_{p,f} (T_{out} - T_{in} - T_{ref}\, ln \frac{T_{out}}{T_{in}}) \tag{4}$$

where T_{ref} is the temperature corresponding to the dead state, which in this work has been taken as 45℃ due to being a reasonable value for the temperature at which the vapor is condensed in the power generation block.

To determine the pressure drop in the packed bed, the Carman correlation is used [24]:

$$\left.\frac{\delta p}{\delta x}\right|_i = \pm\left(\frac{5}{Re_{1,i}} + \frac{0.4}{Re_{1,i}^{0.1}}\right)\frac{6\rho_f v_f^2(1-\epsilon_i)}{d_{p,i}\epsilon_i^3} - \rho_f g \tag{5}$$

$$\text{where } Re_{1,i} = \frac{\rho_f v_f d_{p,i}}{6(1-\epsilon_i)\mu_f} \text{ (spherical particles) and } v_f = \frac{\dot{m}}{\rho_f A_t}$$

In this equation x increases from the bottom to the top, and therefore, the positive sign is used in the discharge of the tank while in the charge process the negative sign is used. The last term accounts for the pressure reduction/increase due to the gravitational action.

For further details of the model used, please refer to reference [18].

2.1.1. Discretization and validation

The diffusive term of Eq. (1) has been discretized using a 2$^{\text{nd}}$ order central difference spatial and a fully implicit temporal integration schemes. The convective term is time-integrated using a fully explicit, 1$^{\text{st}}$ order scheme; and depending on the Péclet number ($\Delta x\, v_f/k_{eff}$), it is discretized either using an upwind scheme (coarser meshes) or a centered scheme (finer meshes), avoiding unboundedness problems on the one side and high numerical diffusion on the other.

The criterion for choosing the time step is similar to that indicated in [18]. If the convective term of the energy equation of the HTF is of higher strength than the diffusive term, a CFL number of 1 is imposed ($\Delta t = \epsilon\Delta x/v_f$). However, if the diffusive term is stronger, the time step is determined by imposing Δt_{diff} = C($\epsilon\rho C_p\Delta x^2/2k_{eff}$) (where C is chosen between 0.5 and 1) for accuracy reasons. It should be noted that for the cases studied within this work, the time steps resulting from this last condition are similar to those obtained by the CFL=1 condition with the tanks operating under the nominal mass flux.

Therefore, when the mesh is coarse enough, the upwind scheme is used for the convective term and the time step is determined by setting CFL = 1. On the other hand, when the grid is fine enough, the diffusive term results in a comparable or (higher) strength than the convective term, in which case, the centered scheme is used and the CFL number is set to be lower than 1. For further details on the discretization procedure please refer to [18].

The validation of the model was performed against two experimental cases, one of a thermocline tank filled with a mixture of Quartzite rock and sand (experimental work of Pacheco et al. [5]) and another of a packed bed of encapsulated PCM (experimental work of Nallusamy et al. [25]). The results of both validation cases are presented in [18]; where a very good agreement was obtained for the first case and also for the HTF temperature profiles of the second case, and some differences with the PCM temperature profiles of the latter were observed. These discrepancies have been attributed to several reasons, such as the model not accounting for the natural convection and contact melting phenomena inside the PCM capsules, and also to uncertainties in the thermo-physical properties of the PCM and in the position of the thermocouples inside the capsules in the experimental setup. In overall, a good agreement has been obtained for the purposes of this work.

2.2. Tank walls, insulation and foundation

The models used for simulating the heat transfer through the tank walls, insulation and foundation are those presented in [26, 27]. A transient 1D heat balance is performed to find the temperature of the tank walls and the insulation in each tank section. For the foundation, a simplified zonal 1D model has been used. More details about the formulation used for these components can be found in references [26, 27].

2.3. Linking the different components

The connection between the different parts of the system (packed bed + HTF, tank walls + insulation, foundation and outdoor conditions; see Figure 1) is performed by the NEST code. This code is a modular object-oriented tool which connects the different models of the different objects through their boundary conditions, allowing independent solution methods for each object (besides their boundary connections). Furthermore, the NEST platform has been designed to work in a parallel computing infrastructure, allowing faster resolution of complex problems.

The resolution algorithm for the cases presented herein is of the Jacobi kind, where each element uses the boundary conditions passed by the connected elements in the previous iteration.

For more insight on the NEST platform, the reader is referred to [20, 26].

3. Cases of isolated TES under nominal conditions

Two levels of analysis are carried out in this work. The first one is developed in this section, consisting in an isolated analysis of the different TES configurations, under specific operating conditions. Therefore, flow inlet conditions are constant (and equal) for both charge and discharge processes, and no thermal losses to the ambient (nor to the walls and foundation) are considered. Thermal performance is evaluated after reaching a periodic state, which is achieved when consecutive charge/discharge cycles result in the same stored/released energy. With this, thermal performance is independent of the initial state of the first charge/discharge cycle.

Different configurations of thermocline tanks are considered by changing the filler material used. Single-solid, single-PCM and MLSPCM configurations are tested and compared against the ideal performance (no thermal losses) of the two-tank system considered as a reference. The dimensions of one tank of the two-tank molten-salt reference system are 13m height by 38m diameter (adopted from those of Andasol 1 facility [28]). Single-tank systems will be firstly designed with these same dimensions, and finally the diameter will be increased for one selected MLSPCM configuration in order to achieve the same thermal storage in the periodic state as with the molten salt system.

TES charge and discharge processes are carried out with molten salt at 390℃ and 290℃, entering through the inlets placed at its top and bottom, respectively. A mass flow of 948 kg/s is assumed, which is the nominal value for Andasol 1 plant [28].

Furthermore, the following operating conditions are assumed:

- Operating time is not fixed but depends on the temperature of the fluid coming out of the tank at each process. Temperature thresholds are imposed to avoid outlet temperatures too cold or too hot to be sent to the receiving equipment (i.e solar field and power block). The temperature ranges between the thresholds and the highest (discharge) or lowest (charge) will be referred to as "admissible" temperature ranges. Each process is stopped when the temperature of the fluid coming out of the tank goes out from these admissible ranges.

  Here, both ranges have been assumed to be 15% of the maximum temperature interval (100℃); i.e. 290-305℃ for the charging process and 375-390℃ for the discharge.

- Ambient losses are neglected [$U_{TC-Sh} = 0$ in Eq. (1)].

- Several consecutive charge/discharge cycles are simulated until a periodic thermal state is reached, i.e. when there is negligible variation of the stored/released energy between consecutive cycles. Since ambient losses are neglected, the same energy that is stored in the charge must be released in the discharge at the periodic state.

Since the admissible temperature intervals for both charge and discharge processes are quite narrow, outlet fluid temperatures for all the cases are very similar. Therefore, a higher operation time is directly related to a higher stored (or released) energy.

In Table 1, a code for each prototype/configuration is defined. The thermocline-like prototypes can be classified according to the filler material/s used as: single-solid (A); single-PCM (B) and multi-layered solid-PCM (C). Percentages between brackets indicate the portion of total height occupied by each filler material. It should be noted that the chosen PCMs are fictitious, having the same thermal properties as those of potassium hydroxide (KOH) but with different fusion temperatures.

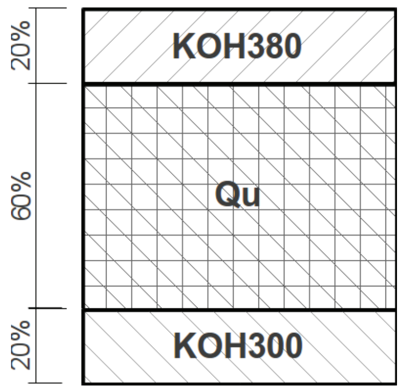

Figure 3: Sketch of MLSPCM prototype C1.

The exception is case B1, where KOH is considered with its actual melting point (360℃ according to [12]). This procedure has been adopted in order to account for the variations in performance exclusively due to the change in the fusion temperature of the PCMs. Figure 3 depicts a sketch of one of the prototypes tested. Table 2 shows the physical properties used in the simulations. The solid filler material adopted here is a mixture of quartzite rock and sand [5]. For the filler material, both PCM and solid, a diameter of 15mm is adopted. Porosity is 0.4 for the PCM layers and 0.22 for the packed bed of quartzite rock and sand. The volume fraction of capsules occupied by PCM is 85%.

Table 1: Codification of prototypes.

Filler material/s[1] - Tank dimensions	Code
2-Tank molten salt - 13m×38m	2-TANK
Quartzite rock & sand (Qu) (100%) - 13m×38m	A1
KOH (100%) - 13m×38m	B1
KOH380 (100%) - 13m×38m	B2
KOH300 (100%) - 13m×38m	B3
MLSPCM: KOH380-Qu-KOH300 (20%-60%-20%) - 13m×38m	C1
MLSPCM: KOH380-Qu-KOH300 (5%-90%-5%) - 13m×38m	C2
MLSPCM: KOH380-Qu-KOH300 (5%-90%-5%) - 13m×43.7m	C3
Quartzite rock & sand (Qu) (100%) - 13m×43.7m	A2

[a]Materials KOHXXX (where XXX is a 3 digit number) are fictitious PCMs with fusion temperatures indicated by the number XXX (e.g. 300℃), whose thermal properties are equal to those of KOH (whose fusion temperature is 360℃). The order in which the materials are indicated is the one in which they are placed inside the tank, from the top to the bottom. Between brackets, the proportion of the tank height occupied by each filler layer is indicated.

Table 3 shows the mass of solid filler material, PCM and HTF contained for each prototype. Due

Table 2: Thermo-physical properties

	Quartzite rock & sand [30]	PCM [12]	Molten Salt [29]
ρ $[kg/m^3]$	2500	2040	1873.8
$C_{p,s}$ $[J/kg\,K]$	830	1340	-
$C_{p,l}$ $[J/kg\,K]$	-	1340	1501.5
k_s $[W/m\,K]$	5.69	0.5	-
k_l $[W/m\,K]$	-	0.5	$0.443 + 1.9 \times 10^{-4} T(^{\text{o}}\text{C})$
μ $[Pa\,s]$	-	-	$22.714 \times 10^{-3} - 0.12 \times 10^{-3} T + 2.281 \times 10^{-7} T^2 - 1.474 \times 10^{-10} T^3$
L $[J/kg]$	-	1.34×10^5	-

to the higher porosity of the PCM layers, the configurations including encapsulated PCMs have a higher amount of confined heat transfer fluid. Furthermore, as the solid filler material is more dense than the PCM, a higher amount of the former results in a higher total mass. The same table also presents data of the storage capacity for each configuration, i.e. the maximum amount of energy that could (theoretically) be stored taking into account both sensible and latent energy contributions, with a temperature jump of 100℃ (290℃- 390℃). In the case of the 2-tank system, the stored energy at the periodic state is equal to the capacity, since this system is not affected by the phenomenon of thermocline degradation and the thermal losses to the ambient are not considered in this part of the study.

3.1. Results and discussion

Table 4 shows the quantitative results obtained from the simulation of the different cases considered, after the periodic steady state has been reached. The different cases (or prototypes) are divided into two groups, one in which the tank dimensions are the same as those of the 2-tank system, and another in which the diameter of the tank is increased.

Results depicted in Table 4 correspond to simulations run with a grid with $N_x = 1040$ and $N_r = 10$. These have been checked to be good in terms of grid independence, since comparing against results obtained with a grid with double resolution (for some cases), the differences in the values of stored energy were lower than 0.6%.

Table 3: Mass confined inside the tank and storage capacity

Mass data (ton)	2-TANK	A1	B1	B2	B3	C1	C2	C3	A2
Mass of PCM	0.0	0.0	13013.4	13013.4	13013.4	5205.4	1301.3	1721.0	0.0
Mass of solid filler material	0.0	28749.8	0.0	0.0	0.0	17249.9	25874.8	34219.5	38021.6
Mass of confined HTF	27629.3	6078.4	11051.7	11051.7	11051.7	8067.8	6575.8	8696.5	8038.7
Total mass	27629.3	34828.3	24065.2	24065.2	24065.2	30523.0	33752.0	44637.0	46060.4
Storage Capacity									
Filler material (MWh)	0.00	662.84	968.78	968.78	968.78	785.22	693.44	917.07	876.61
Confined HTF (MWh)	1152.36	253.52	460.94	460.94	460.94	336.49	274.26	362.71	335.28
Total (filler+HTF) (MWh)	1152.36	916.36	1429.72	1429.72	1429.72	1121.71	967.70	1279.78	1211.89
Total sensible energy (%)	100.0	100.0	66.1	66.1	66.1	82.7	95.0	95.0	100.0
Total latent energy (%)	0.0	0.0	33.9	33.9	33.9	17.3	5.0	5.0	0.0

3.1.1. Prototypes with tank dimensions of 13m × 38m

Cases A1 to C2 correspond to different thermocline configurations of tanks with the same dimensions as that of a single tank of the 2-tank system (13m × 38m).

As seen in previous works [18, 19], the single-solid-filled thermocline tank shows a degradation of the thermocline throughout consecutive charge/discharge cycles, due to the restrictions on the outlet fluid temperature. As a result, the stored energy at the periodic state is around 80% of its storage capacity. This value is higher than that obtained for the small scale prototype tested in [18] (with dimensions of 5.2m × 3m), where a utilization of around 63% of the capacity was obtained. The reason for this is that the thermocline height in both cases is similar —around 2m in the case of [18] and 3m in the present case (see fig. 4)—while the height of the tank is very different, resulting in a lower thermocline zone relative to the height for the case presented here ($\sim$ 23% vs. $\sim$ 33.3%).

Table 4: Performance results for each configuration

	Diameter = 38m							Diameter = 43.7m	
Results	2-tank	A1	B1	B2	B3	C1	C2	C3	A2
Operation time (h)[1]	8.10	5.18	3.06	6.61	6.61	7.12	6.43	8.54	6.88
Stored Energy in Filler material (MWh)	0.0	529.7	226.6	501.6	501.5	659.2	645.8	857.7	703.4
Stored Energy (Filler + confined HTF) (MWh)	1152.4	732.7	432.4	902.6	902.5	937.6	894.6	1188.7	972.9
Stored Energy / Storage capacity (%)	100.0	80.0	30.2	63.1	63.1	83.6	92.4	92.9	80.3
Stored Energy / Stored Energy in 2-tank (%)	100.0	63.6	37.5	78.3	78.3	81.4	77.6	103.2	84.4
Sensible energy stored / Total stored (%)	100.0	100.0	97.4	90.9	90.9	80.5	94.8	94.8	100.0
Latent energy stored / Total stored (%)	0.0	0.0	2.6	9.1	9.1	19.5	5.2	5.2	0.0
Effective mass of PCM changing phase (%)	-	-	2.3	16.9	16.9	94.3	95.3	96.0	0.0
Exergy difference at charge (MWh)	-553.2	-352.0	-207.7	-433.4	-436.2	-453.2	-430.3	571.8	-467.4
Exergy difference at discharge (MWh)	553.2	351.6	207.3	430.54	433.3	447.3	428.7	569.7	466.8
Exergy at discharge / Exergy at discharge of 2-tank (%)	100.0	63.5	37.5	77.8	78.3	80.9	77.5	103.0	84.4
Pumping energy / Stored Energy (%)	0.08	0.09	0.09	0.09	0.09	0.09	0.09	0.09	0.09

[a]In cases where the charge and discharge operation times are different, (e.g. B2 and B3) the mean value between processes is shown.

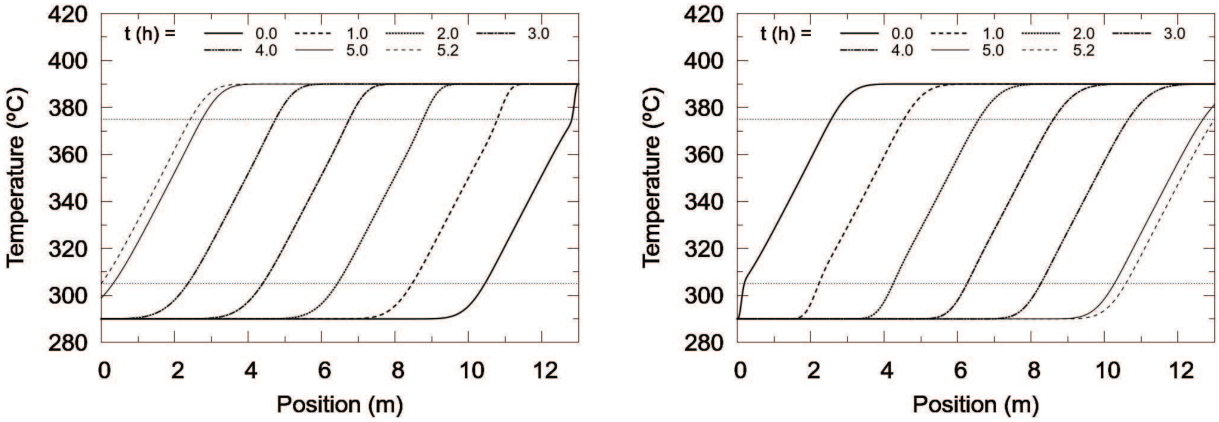

(a) Charge

(b) Discharge

Figure 4: Case A1. Periodic state. Temperature maps at various instants. The chronological order of the curves is from right to left for the charge process and from left to right for the discharge. Horizontal dotted lines indicate the threshold temperatures.

Case A1 results in both delivered energy and exergy to the PB of ∼64% with respect to the obtained with the 2-tank system.

Prototype of case B1 is filled with a single encapsulated PCM with a fusion temperature of 360℃ (KOH) which is outside both admissible temperature ranges for the outgoing fluid. The thermal performance of the prototype filled with this encapsulated PCM is the worst of all the cases studied.

The percentage of PCM effectively changing phase between processes is very low (2.3%) and also the usage of the storage capacity (30%).

Figure 5 shows the temperature maps for the periodic state. It can be observed that the area between the initial and last temperature curves is very small, resulting in a very low utilization of the sensible energy capacity of the system.

As observed in [18], the reason for this poor performance is that the melting point is not within any of both admissible temperature ranges. In the charging phase, the phase-changing zone (at 360℃) advances from the top of the tank to the bottom. Beyond this zone, both the fluid and filler materials are at a lower temperature, and thus, no melting of the PCM is occurring. At the begining of the charge, the temperature of the outflow is 290℃ but starts increasing after a while, when the hotter upstream fluid gets to the outlet. This continues until the threshold of 305℃is reached, when the charging process stops. At this point, a high portion of the PCM is at temperatures lower than the melting point (between 305-360℃), and therefore, has not absorbed energy in the form of latent heat. This portion of PCM (close to the bottom of the tank) is not able to release latent heat to the HTF in the subsequent discharge; where moreover, the PCM closer to the top is not able to solidify due to being at a temperature range between 360-375℃, at the end of the process. Therefore, at the periodic equilibrium state, only a small portion near the middle zone of the tank effectively changes phase from one process to the next, resulting in a very low utilization of the latent heat capacity of the PCM. Furthermore, the sensible capacity is also very poorly used, due to the limitation imposed by the phase-changing PCM to the range of temperatures allowed to the materials contained at both sides of it (between 290-360℃ for the cold zone and between 360-390℃ for the hot zone).

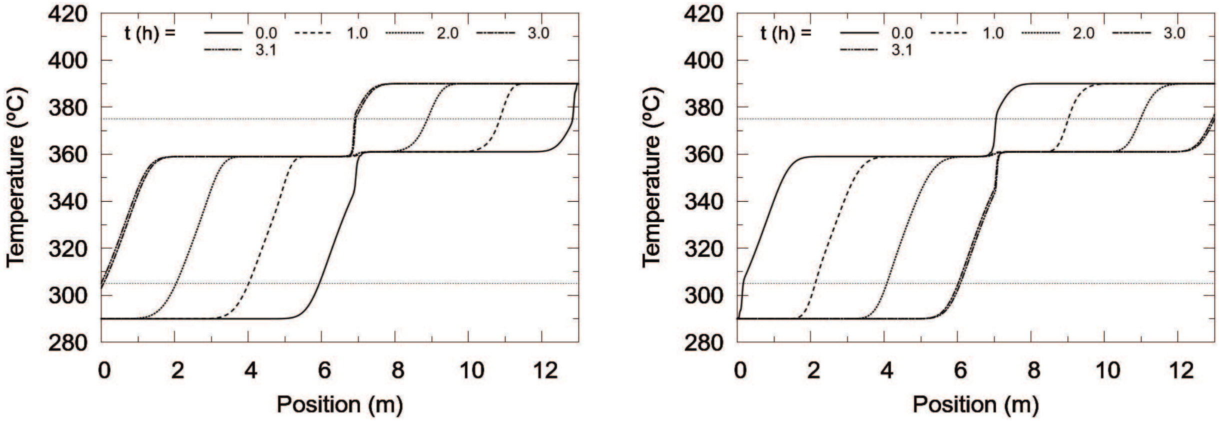

(a) Charge (b) Discharge

Figure 5: Case B1. Periodic state. Temperature maps at various instants. The chronological order of the curves is from right to left for the charge process and from left to right for the discharge. Horizontal dotted lines indicate the threshold temperatures.

Cases B2 and B3 have the common feature of using PCMs whose melting points lie inside each of the admissible temperature ranges. Temperature maps for the periodic state of both cases are shown in figures 6 and 7. A first observation is that the area between the initial and final maps for both cases is significantly higher than that of case B1. As a result, a higher utilization of the storage capacity, and thus, a higher stored energy, is obtained with these prototypes. Due to the symmetry between key temperatures of cases B2 and B3 (melting points, thresholds and operating range), the resulting temperature maps for the periodic state are also symmetric and the thermal performance results for both cases are almost identical. It can be observed that the efficiency in the use of the phase change material and of the whole storage capacity are much higher than that of prototype B1, but not yet ideal (17% and 63%, respectively, for both B2 and B3). In these cases, the PCM located close to the outlet corresponding to the process whose admissible range contains the melting point (the one in the top for case B2 and the one in the bottom for case B3), act as a thermal buffers by not allowing the outflow temperature to escape from the admissible range, until it has changed phase. In the subsequent process, this portion changes phase again, since it is the first to encounter the cold/hot fluid coming through the inlet. Therefore, a higher portion of PCM effectively changes phase in the periodic state, also allowing a higher use of the sensible energy capacity of the PCM which does not melt/solidify.

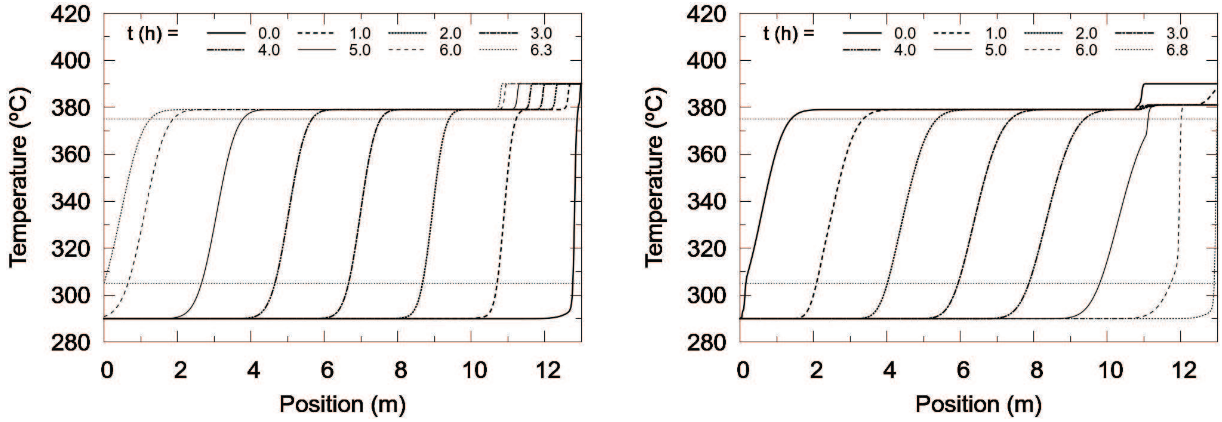

(a) Charge (b) Discharge

Figure 6: Case B2. Periodic state. Temperature maps at various instants. The chronological order of the curves is from right to left for the charge process and from left to right for the discharge. Horizontal dotted lines indicate the threshold temperatures.

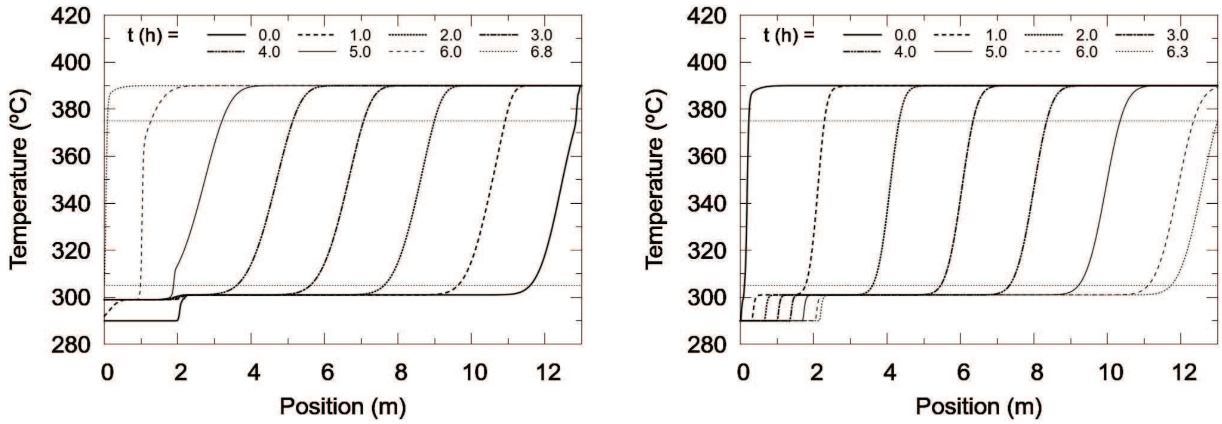

(a) Charge (b) Discharge

Figure 7: Case B3. Periodic state. Temperature maps at various instants. The chronological order of the curves is from right to left for the charge process and from left to right for the discharge. Horizontal dotted lines indicate the threshold temperatures.

Cases C1 and C2 are MLSPCM configurations with only two different PCMs collocated at both extremes of the tank and a solid filler material (quartzite rocks & sand) in the middle zone, forming a 3-layer arrangement, only differing in the width of the layers. Figure 3 shows a sketch of the configuration of prototype C1. Due to the symmetry of the operating conditions, the design of the filler materials configuration is also symmetric. The PCMs used are those whose melting points are contained in the admissible temperature ranges for the outgoing fluid in both processes, KOH380 and KOH300.

In [18], it was observed that only the energy contained in the HTF between the inlet temperature and the melting point of the PCM located at the inlet can be "used" for producing the phase-change of the PCM, at most. This is, in the charge process, only the energy contained between 390℃ (inlet) and 380℃ is available for melting the PCM layer of KOH380 (located at the top). Therefore, as only 10-12% of the whole energy available to be stored can be used for producing the phase-change of each PCM layer, then only 20-24% of the energy can be stored/released in the form of latent energy. Hence, in order to assure that most of the PCM will effectively undergo a change of phase, configurations with a latent energy capacity of less than 20% are considered here. Observe, from Table 3, that prototype C1 has a latent energy capacity of 17% of the total storage capacity and this value is only 5% in C2.

Performance results of these two cases, are the best in terms of efficiency in the use of the storage capacity (C1 84%, C2 92%) and in the use of the latent energy (94-95% of the PCM changing phase between processes). In terms of total energy and exergy delivered, their results are similar to those obtained in cases B2 and B3, with around 78-81% of those obtained in the 2-tank system. All this is possible with the use of a relatively small amount of encapsulated PCM, being most of the tank filled with the cheaper solid material.

Figures 8 and 9 show the temperature maps after reaching the periodic state, where the thermal buffering effect of the PCMs collocated at both ends of the tank can be observed. In each process, phase changing capsules located close to the fluid outlet, force the temperature of the outgoing HTF to remain close to the PCM melting point, and thus, inside the corresponding admissible range. This allows a longer operating time and a higher thermal filling of the whole tank.

Regarding the pressure losses produced by the presence of the filler material, it can be seen that they are negligible (less than 1% of total pressure losses). Pumping energy needed to overcome these, plus the gravitational force, represent less than 0.1% of the stored energy for all cases.

In summary, compared against solid-filled thermocline design, MLSPCM concept present higher storage capacity together with a higher efficiency in its utilization. Furthermore, although presenting lower overall capacity, MLSPCM prototypes yield a much higher efficiency than single-PCM ones, resulting in similar values of total energy storage.

3.1.2. Prototypes with larger diameter (13m $\times$ 43.7m)

Prototype C2 is probably the most cost-effective among those including encapsulated PCMs, due to its high efficiency and low amount of PCM used. However, in order to yield the same values of

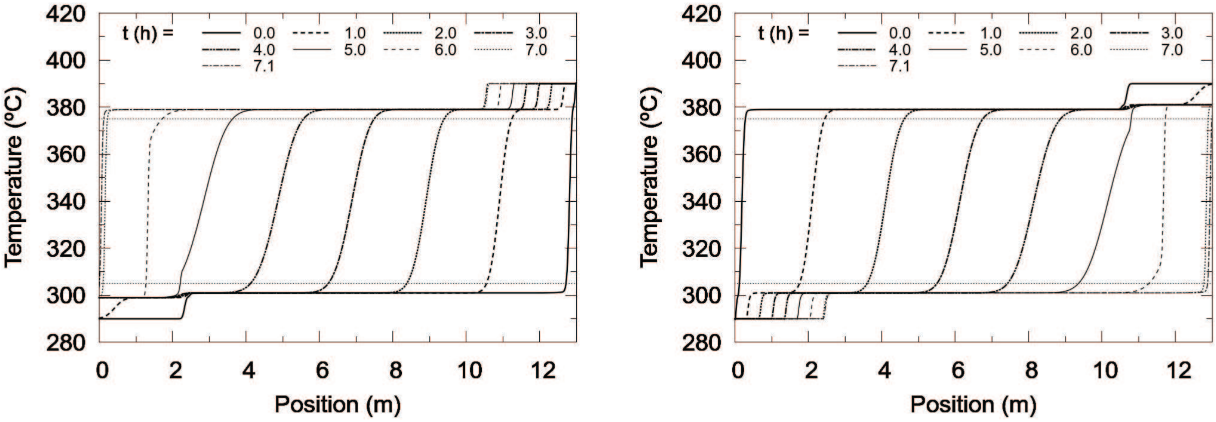

(a) Charge **(b)** Discharge

Figure 8: Case C1. Periodic state. Temperature maps at various instants. The chronological order of the curves is from right to left for the charge process and from left to right for the discharge. Horizontal dotted lines indicate the threshold temperatures.

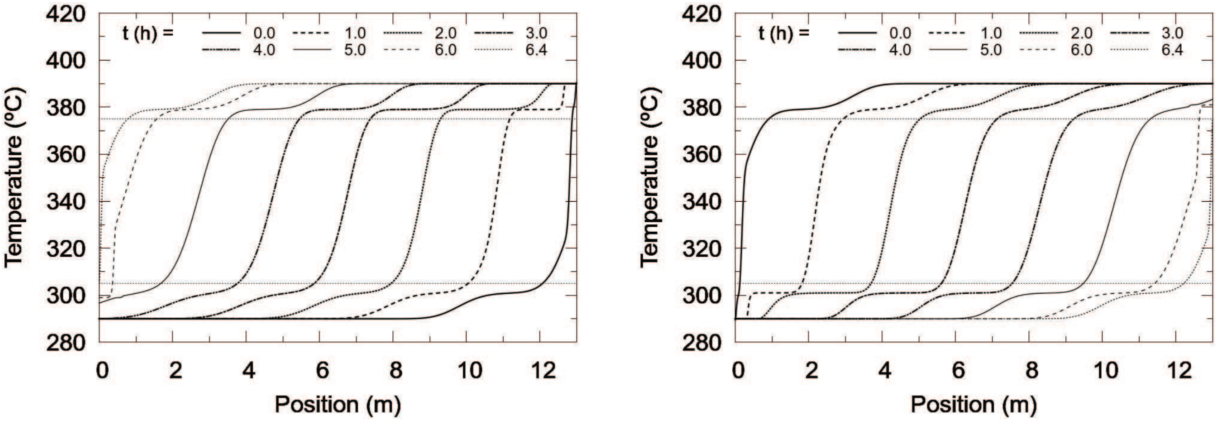

(a) Charge **(b)** Discharge

Figure 9: Case C2. Periodic state. Temperature maps at various instants. The chronological order of the curves is from right to left for the charge process and from left to right for the discharge. Horizontal dotted lines indicate the threshold temperatures.

energy —and more precisely, exergy — delivered to the power block as those of the 2-tank molten-salt system, the storage capacity of the single-tank system has to be increased. Hence, the tank diameter is enlarged.

Case C3 corresponds to this new case, with a tank diameter of 43.7m, where thermal performance values can be seen to be very similar to those of the ideal 2-tank system. The stored/released energy and exergy delivered to the PB are around 3% higher than with the 2-tank, while the efficiencies in the use of the total and latent capacities are very high.

This prototype has a volume 32% higher than one tank of the 2-tank system and requires around

68% less amount of molten salt than the latter. On the other hand, it needs to hold around 62% more weight and requires two small layers of encapsulated PCM (with less than 4% of total weight).

Case A2, which has the same tank dimensions as C3 but is totally filled with solid material, results in an effective storage of around 84% with respect to that of the 2-tank system and around 82% with respect to the obtained with C3.

Figures 10 and 11 depict the temperature maps of these two cases in the periodic state. It can be observed how the inclusion of the PCM layers induce a higher utilization of the sensible energy capacity of the tank, as already observed between cases A1 and C2.

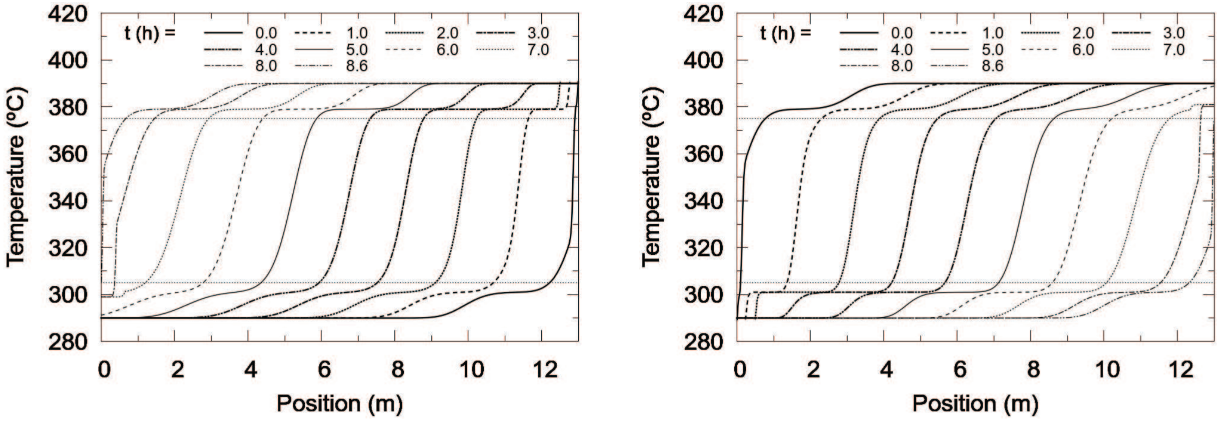

(a) Charge **(b)** Discharge

Figure 10: Case C3. Periodic state. Temperature maps at various instants. The chronological order of the curves is from right to left for the charge process and from left to right for the discharge. Horizontal dotted lines indicate the threshold temperatures.

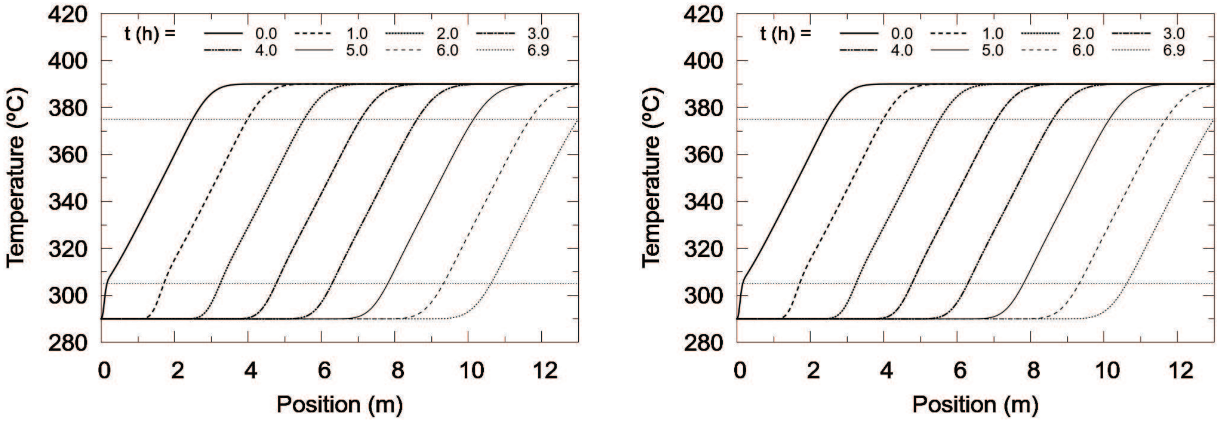

(a) Charge **(b)** Discharge

Figure 11: Case A2. Periodic state. Temperature maps at various instants. The chronological order of the curves is from right to left for the charge process and from left to right for the discharge. Horizontal dotted lines indicate the threshold temperatures.

In summary, a single-tank TES system equivalent to the reference 2-tank system, results smaller and more efficient when using an appropriate MLSPCM configuration than when using a solid-filler material.

4. Cases of TES integrated into a CSP facility

In this section, the analysis of the TES systems integrated into a CSP facility is performed, by taking into consideration the variations of the direct normal irradiation (DNI) on the solar field (SF), as well as the thermal energy losses to the ambient through the tank shell and foundation. Furthermore, idle processes are simulated; i.e. when there is no fluid flow through the tank.

The parameters for the reference CSP plant are shown in Table 5. The heat transfer fluid passing through the TES is molten salt. A sketch of the plant with a single-tank TES is shown in Fig. 12. The thermo-physical properties of the different materials in the packed beds are the same used for the previous cases. The efficiency of the heat exchanger intended to transfer heat between the fluids from the SF and TES is assumed to be 1.

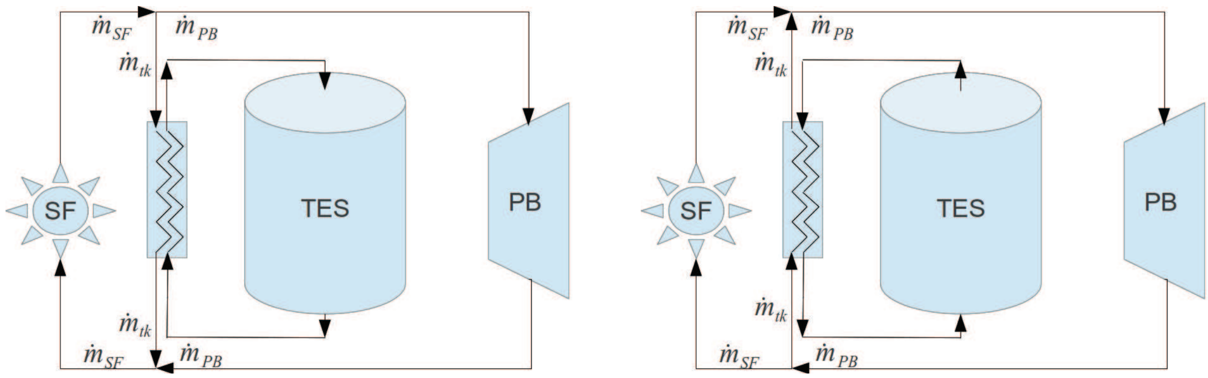

(a) Charge **(b)** Discharge

Figure 12: Sketch of CSP plant with single-tank TES.

4.1. Operating conditions

The same values of temperature of fluid coming from the solar field and from the power block (PB) as those of section 3 are adopted here, 390°C and 290°C, respectively. Furthermore, the same admissible temperature ranges are here considered, i.e. 375-390°C for the discharge and 290-305°C for the charge. However, one difference between the criterion used here and the one used in section 3 is that the temperature limits are not applied to the fluid flows coming out of the TES directly. Instead, the controlled temperature is that of the fluid coming into both, the SF and the PB. Hence, if the TES is being charged and the PB is generating power simultaneously, the fluid entering the SF is a

Table 5: Parameters of reference CSP plant

Turbine nominal power (MWe)	50
Solar field technology	Parabolic trough
Solar field area (m^2)	510120
Solar field peak efficiency (%)	70
Power block peak efficiency (%)	38
Storage capacity w/ 2-tank system (MWhth)	1152

mixture of the fluid streams coming from the PB and from the TES heat exchanger (see the sketch in Fig. 12a), and therefore, its temperature is not that of the cold fluid coming out of the TES but a weighted average of the temperatures of both streams. Something similar occurs with the temperature of the flow going to the PB if the TES is discharged at the same time as the SF is collecting heat (see the sketch in Fig. 12b). Therefore, the current criterion is less restrictive, from the point of view of the TES, since the temperature of the fluid coming out of it could be outside the corresponding admissible range but the process would not be stopped, as long as the temperature of the fluid coming into the receiving equipment still remains inside this range.

To avoid several charge and discharge processes being started and stopped in small time intervals, different (more restrictive) thresholds have been defined for starting the processes; i.e. a discharge is not initiated if the temperature at the top of the tank is lower than 380℃, while a temperature at the bottom of the tank higher than 300℃ is required for charging the tank.

The initial conditions for the TES, in the first day of simulation, are uniform temperatures of 290℃ for the whole tank and 15℃ for the soil.

The simulations are carried out for 17 days in summer (from June 30 to July 17) in Seville, Spain. The direct normal irradiation (DNI) and the rest of weather data are obtained from METEONORM software version 4.0. Table 6 depicts some basic information for this location.

For determining the power coming from the solar field, the following equation is used:

$$\dot{Q}_{SF} = DNI \times A_{SF} \times \eta_{SF}$$

where the DNI is multiplied by the surface area (A_{SF}) and overall efficiency of the solar field (η_{SF}), which is taken as the peak efficiency of the solar field in Andasol 1 plant [28] (see Table 5). It is assumed that the mass flow coming from the solar field is directly sent to the power block until the nominal power is reached, then, the excess flow is used to charge the storage system. When the mass flow from the SF is not enough to reach the nominal electric power, the TES discharge starts and the mass flow passing through the heat exchanger, placed between the SF and TES, is calculated as the difference between the mass flow coming from the SF and that needed for generating nominal power in the PB. The discharge continues until the threshold temperature is reached ($T_{PB} < 375$ ℃). After this, an idle process takes place until there is excess energy available to charge again the storage system.

The nominal thermal power, from the point of view of the TES, is calculated as:

$$\dot{Q}_{PB,nom} = \frac{\text{Nominal power}}{\eta_{PB} \times 0.98} = 134.26 \text{ MW}$$

where 0.98 is the assumed efficiency of the heat exchanger of the PB (not shown in figure 12) and η_{PB} is the efficiency of the PB (see Table 5).

From this value, the nominal molten salt mass flow passing through the TES is calculated as:

$$\dot{m}_{HTF,nom} = \frac{\dot{Q}_{PB}}{C_{p,HTF} \times \Delta T_{HTF}} = 894.2 \text{ kg/s} \tag{6}$$

where ΔT has been taken as 100℃ (290-390℃). This value is a little lower than the one used in section 3 (948 kg/s), which corresponds to that of Andasol 1 plant according to [28]. Therefore, $\dot{m}_{HTF,nom}$ is the mass flow passing through the TES in the discharge, when there is no available energy from the SF.

Table 6: Location basic data

			July		
Location	Latitude (º)	Longitude (º)	T_{max} (℃)	T_{min} (℃)	DNI (kWh/m^2 day)
Seville, Spain	37.37	5.97	39.6	16.2	7.58

In figure 13, the curves of thermal power coming from the SF, thermal power needed to generate the nominal (electric) power in the PB and the remaining thermal power available to be stored in the TES, are plotted for the time range of the simulations.

4.2. Tank configurations

The same configurations tested in the simplified case (Table 1) are here tested, with the addition of the tank shell, insulation and foundation.

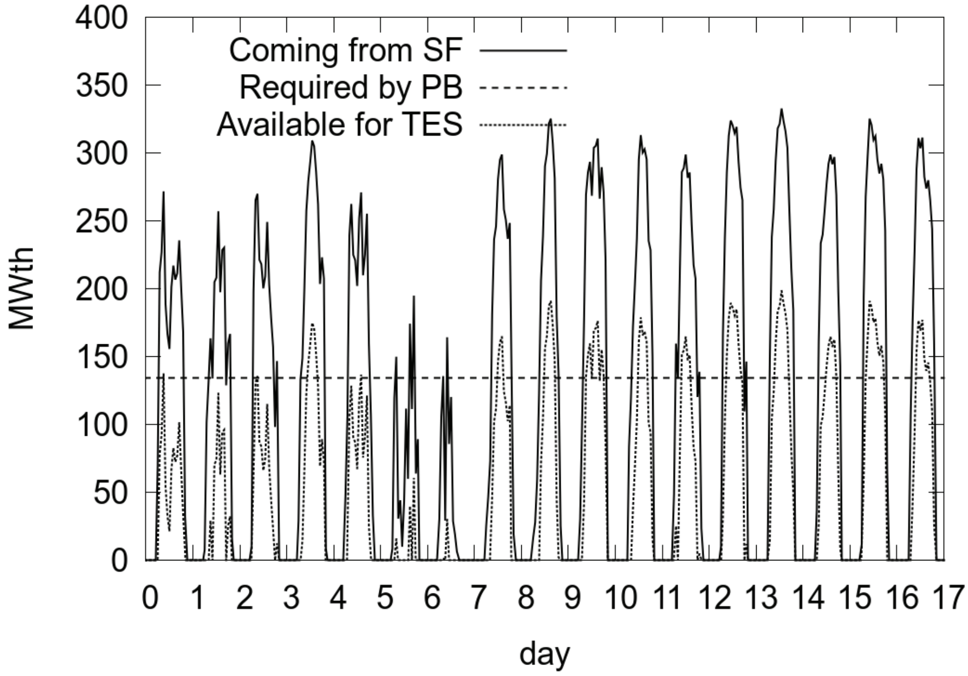

Figure 13: Thermal power (in MW) coming from the solar field, required by the power block (for nominal power generation) and available for storage, in the 17 days of simulation.

The tanks are made of steel A516gr70, while the insulation material for the lateral wall and roof is Spintex342G-100. The insulation is covered with a thin layer of aluminum 2024 T6.

Common geometric parameters for all the cases:

- Vertical wall thickness = 0.039 m.
- Bottom wall thickness = 0.021 m.
- Insulation thickness = 0.4 m.
- Foundation thicknesses: dry sand = 0.006 m; foam-glass = 0.420 m; heavy weight concrete = 0.450 m; soil = 9.140 m.

The thermo-physical properties of all the used materials can be found in [26].

4.3. Results and discussion

Table 7 shows the results for all the presented cases, which are expressed as mean values, per day, of the 17 days of simulation.

Firstly, it can be seen that the reference 2-tank TES shows zero energy losses, due to being considered as the ideal case, i.e. the hot tank is always at 390°C and the cold tank at 290°C. However, the storage capacity is not entirely used because of the fact that not in some days there is not enough available energy (from the SF) to fill the 2-tank system completely. On the other hand, in some days there is an excess of energy and some has to be discarded (see the “unused available energy” row in Table 7), probably by defocusing some collector lines in the solar field.

In the last row of Table 7, the number of days for which the temperature threshold is reached by the outlet fluid in the charging process is presented. This can be seen as the number of days in which the effective thermal capacity is exhausted. The term “effective” is used in order to differentiate between the capacity indicated in Table 3, which is the ideal capacity and does not depend on the temperature thresholds, and the “real” one which is the one that results from the simulations with the restrictions in the outlet temperature. In the case of the 2-tank, since the threshold is never reached, the number of days in which the system is totally charged is indicated.

The fact of not exhausting the effective capacity in every day of simulation distinguishes the present operating conditions from those of section 3, since in the latter the charge was not stopped until the temperature threshold was reached.

The differences in the values of total energy coming from the SF and available energy for storage, between the different prototypes, is due to interpolation errors of the input data. These are available at intervals of one hour and are needed for each time step of simulation, with a frequency in the order of seconds and dynamically determined by the code, resulting in different interpolation steps for each case.

Table 7: Performance results for each configuration.

	Diameter = 38m							Diameter = 43.7m	
Results	2-tank	A1	B1	B2	B3	C1	C2	C3	A2
Total energy from SF (MWh)	2798.6	2776.3	2776.1	2776.1	2780.8	2776.3	2776.3	2776.6	2776.3
Energy available for charging the TES (MWh)	1151.0	1125.8	1126.2	1126.1	1126.2	1125.8	1125.8	1125.8	1125.8
Energy delivered to the PB by the TES (MWh)	959.4	715.3	397.0	794.6	762.4	805.7	777.3	963.6	879.0
Energy delivered by TES / TES capacity (%)	83.3	78.1	27.8	55.6	53.3	71.8	80.3	75.3	72.5
Energy delivered by TES / Delivered by 2-tank (%)	100.0	74.6	41.4	82.8	79.5	84.0	81.0	100.4	91.6
Energy losses (MWh)	0.0	3.4	3.6	3.3	3.4	3.4	3.4	4.2	4.3
Energy losses / Energy delivered to PB by TES (%)	0.0	0.4	0.9	0.4	0.4	0.4	0.4	0.4	0.5
Exergy delivered to the PB by the TES (MWh)	460.6	343.2	190.3	379.1	365.7	384.4	372.4	461.6	421.7
Exergy Delivered/ Delivered by 2-tank (%)	100.0	74.5	41.3	82.3	79.4	83.5	80.8	100.2	91.5
Unused available energy (MWh)	191.6	402.9	692.1	221.7	330.5	311.3	342.9	154.8	236.1
Nº of days in with the charge is stopped by threshold	10[1]	13	14	12	12	12	12	9	11

[a]Temperature thresholds are never reached by the 2-tank TES, and therefore, the number of days correspond to those when the system is totally charged.

For the solid-filled thermocline prototype A1, the values of energy and exergy delivered to the PB are lower than those obtained with the 2-tank (74.5%). However, these differences are not as high as those shown in section 3. This is in part due to the variability of the available energy for storage, which in some days is lower than the storage capacity, and also to the less restrictive operating conditions for the TES (mentioned above), which allow a greater thermal filling than that allowed in section 3. Figure 14 shows the initial and final temperature maps for charge and discharge processes in the 10^{th} day, with durations of more than 6 hours each. It can be observed that the final temperature at the charge goes beyond the threshold (305°C) due to the mixing effect mentioned before, and that the tank is thermally filled to a higher extent than in section 3 (compare with Fig. 4). The difference between the temperature maps at the end of the charge and at the start of the discharge is because an idle process of around 5.5 hours and another charge of around 18 minutes occur between them. Comparing the number of days in which the storage tank "effective" capacity is exhausted, it is observed that this happens in 10 days for the 2-tank system and in 13 for A1. As mentioned above, this explains why the efficiency in the use of total capacity is closer between the 2-tank and A1 prototypes than in section 3, where all the prototypes were charged until reaching the threshold temperature.

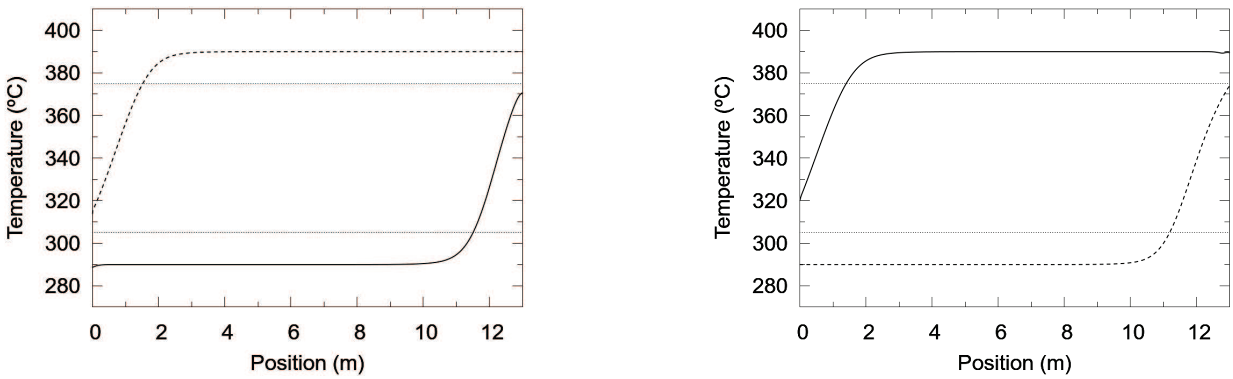

(a) Charge

(b) Discharge

Figure 14: Temperature maps of day 10 for charge and discharge processes for prototype A1. Solid line indicates the temperature at the start of the process and dashed line at the end. Horizontal dotted lines indicate the threshold temperatures.

For prototype B1, the results are much worse, being in agreement with those obtained previously. Similarly as in section 3, the results for prototypes B2 and B3 are much better than for B1 and comparable to those of C2, in terms of total energy and exergy delivered, but worse than the latter in terms of efficiency.

MLSPCM prototypes C1 and C2 result in a storage of around 84% and 80% compared to the 2-tank, respectively. Their efficiency in the use of total capacity is lower than that obtained in section

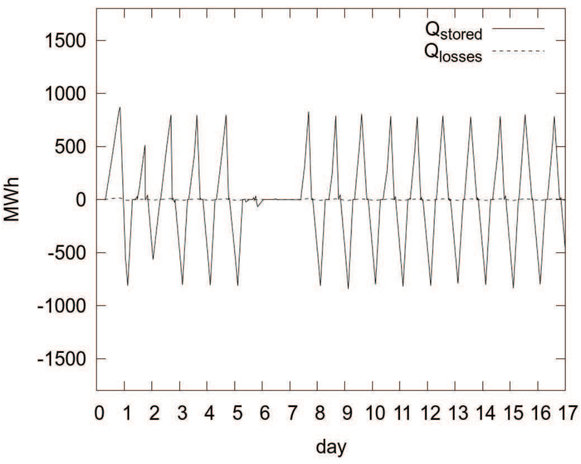

(a) A1

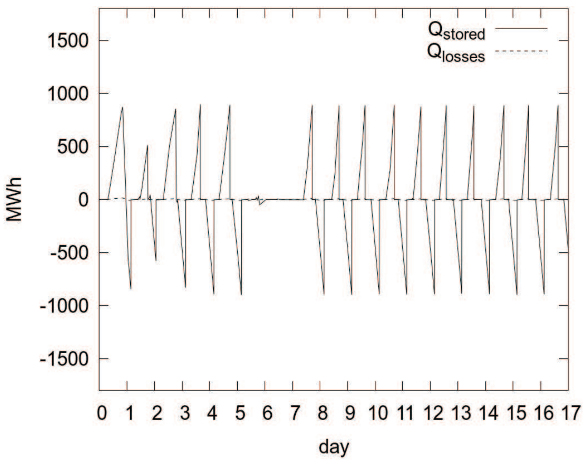

(b) C2

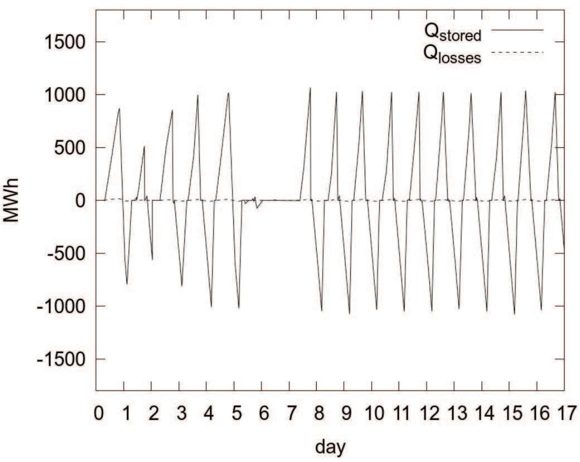

(c) A2

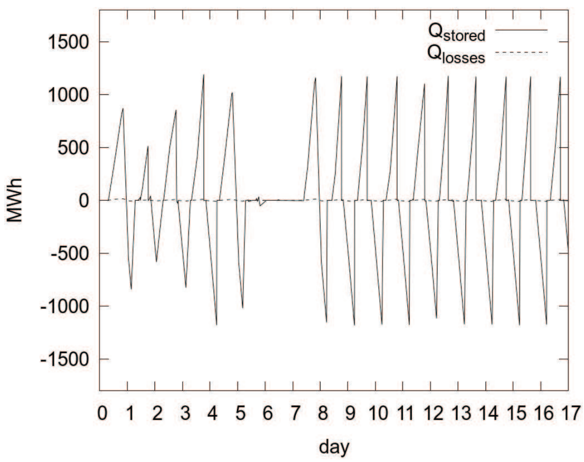

(d) C3

Figure 15: Evolution of the energy stored and lost for several prototypes. Values are reset to 0 at the end of each process. Stored energy (continuous line) has positive values in the charge and negative values in the discharge. Thermal losses (dashed line) are positive when heat comes out of the packed bed (by conduction through the walls) and negative when it comes into it.

3, which again, is mostly due to the occurrence of days of low radiation in which the available energy is not enough to fill the TES. The total energy effectively stored is closer to that obtained by prototype A1, although still higher. C2 still results in a higher use of the storage capacity than A1, but C1 shows a lower value.

Prototype C3, which has the same configuration as C2 but with a higher diameter, is seen to result in almost the same amount of exergy delivered to the power block as in the 2-tank system, and therefore it is considered as equivalent to the latter, since it would result in almost the same amount of power generation. When comparing energy efficiencies of prototypes C3 and A2 it can be observed that it is higher in the former than in the latter (75.3% vs 72.5%), but similar. Case A2 delivers

91.5% of the exergy delivered by the ideal 2-tank. This is 9% lower than that achieved by the C3 configuration, which makes use of the latent heat capacity of the PCM layers.

In Fig. 15, the energy stored and lost for prototypes A1, C2, A2 and C3 are plotted for each day. It can be seen that in the first days there is a significant variation of stored/delivered energy and from the 8th day on, it is stabilized. This is due, on the one hand, to the particular initial conditions of the first day (uniform low temperature), and on the other, to the DNI variations in the first seven days. Particularly, in days 6 and 7 all the TES remain uncharged due to the low amount of available irradiation.

In all cases, the thermal losses are very low (less than 1% of the energy delivered to the PB by the TES for all the cases, and around 0.5% for most), which is an indication of having enough thermal insulation. Due to the transient operation of the tanks, in the discharge processes heat comes into to the packed bed through the tank walls and foundation instead of coming out, and therefore, these components act as additional thermal storage media.

5. Conclusions

MLSPCM thermocline-like thermal energy storage prototypes have been designed for their utilization in a CSP plant. A parabolic trough plant of 50MWe, similar to Andasol 1 (Granada, Spain), has been adopted as reference. The analysis has been carried out using verified and validated models of the thermocline-like configurations, tank walls and foundation.

Two different analyses were performed, one centered in evaluating the performance of the TES systems under specific conditions, in which the TES is charged and discharged consecutively until reaching a periodic steady state; and another in which the same TES configurations are tested under 17 days of operation in the reference CSP plant. In the latter case, weather conditions of Seville (Spain) were adopted, the variation of the operating conditions due to the changes in the direct normal irradiation were simulated, and the tank walls and foundation were taken into account.

MLSPCM single-tank systems, with the same tank dimensions as one of the two-tank molten salt tanks, were compared to the latter system as well as to other single-tank configurations. Furthermore, one of the MLSPCM configurations was chosen for designing a bigger tank, aimed to achieve the same amount of energy stored as that of the two-tank system.

The first analysis confirms the conclusions taken in previous works [18, 19], indicating that MLSPCM configurations diminish the degradation of the thermocline of single-tank solid-filled designs, produced by the restrictions in the outflow temperature. Hence, both total capacity and the extent at which it is harnessed are increased. Compared against single-PCM packed beds, MLSPCM designs yield a much higher efficiency in the use of total capacity, especially when the amount of PCM effectively changing phase is evaluated. Compared against the two-tank system, MLSPCM prototype C3 is considered as its equivalent in terms of energy and exergy delivered to the power block, with a volume 32% higher than that of one of the two tanks and needing only 32% of the amount of molten-salt. On the other hand, the total weight hold by C3 is 62% higher and it needs a relatively small amount of PCM (less than 4% of total weight). If the comparison is performed against a single-solid filled thermocline tank with the same dimensions (i.e. prototype A2), C3 stores around 20% more energy/exergy, holding almost the same weight (around 3% less) and needing around 8% more molten-salt, besides the extra PCM layers.

The second analysis, incorporating more aspects related to the operation of the CSP plant, result in lower differences between the performance of MLSPCM and single-solid thermocline configurations. On one hand, the restrictions on the temperature of the heat transfer fluid are not applied to the flow coming out of the TES, but to that entering the solar field or the power block. This change results in less restrictive operating conditions for the TES, and therefore, the thermocline degradation occurring in the single-solid filled thermocline is not so high. Furthermore, the fact of having days of low radiation result in a penalization of the capacity factor of the systems with higher capacity. Nevertheless, in this analysis, the MLSPCM prototypes tested still show higher values of stored energy/exergy and efficiency (C2 and C3) than single-solid thermocline tanks. When compared against the reference 2-tank system, prototype C3 is still considered equivalent to it, since the values of stored energy and exergy are almost exactly the same. In these conditions, prototype A2 delivers around 10% less energy/exergy to the power block than C3 in the 17 days of simulation.

Thermal losses to the ambient are observed to be very low for all the cases (less than 1%), and the tank walls and foundation act as extra thermal storage media.

As in previous works, MLSPCM concept shows to be a promising alternative to the other TES configurations tested —due to the combination of higher storage capacity and higher efficiency in its use— as well as to the standard two-tank system.

However, variability of operating conditions are seen to affect the relative advantage of using one or another TES system, and therefore, it is possible that TES designs which are optimal for the isolated conditions are not so for the real application. Optimization of MLSPCM designs to one or another CSP facility needs to be studied in further detail, with long-term simulations incorporating all the relevant aspects, such as the real limitations for the HTF temperature, the different thermo-physical properties of the available PCMs and an economic evaluation.

Acknowledgments

This work has been financially supported by the *Ministerio de Economía y Competitividad, Secretaría de Estado de Investigación, Desarrollo e Innovación*, Spain (ENE-2011-28699), by the EIT via the KIC InnoEnergy TESCONSOL project (ref. 20_2011_IP16) and by the *Secretaria d'Universitats i Recerca (SUR) del Departament d'Economia i Coneixement (ECO) de la Generalitat de Catalunya* and by the European Social Fund.

References

[1] M. Medrano, A. Gil, I. Martorell, X. Potau, and L. F. Cabeza, "State of the art on high temperature thermal ebergy storage for power generation. part 2—Case studies," *Renew. Sust. Energ. Rev.*, no. 14, pp. 56–72, 2010.

[2] G. J. Kolb, C. K. Ho, T. R. Mancini, and J. A. Gary, "Power tower technology roadmap and cost reduction plan," Tech. Rep. SAND2011-2419, Sandia National Laboratories, 2011.

[3] U. Herrmann, B. Kelly, and H. Price, "Two-tank molten salt storage for parabolic trough solar power plants," *Energy*, vol. 29, pp. 883–893, 2004.

[4] J. I. Ortega, J. I. Burgaleta, and F. M. Téllez, "Central receiver system solar power plant using molten salt as heat transfer fluid," *J. Sol. Energ.-T. ASME*, vol. 130, pp. 024501–1–6, 2008.

[5] J. E. Pacheco, S. K. Showalter, and W. J. Kolb, "Development of a molten-salt thermocline thermal storage system for parabolic trough plants," *J. Sol. Energ.-T. ASME*, vol. 124, pp. 153–159, 2002.

[6] A. Yang and S. V. Garimella, "Molten-salt thermal energy storage in thermoclines under different environmental boundary conditions," *Appl. Energ.*, vol. 87, pp. 3322–3329, 2010.

[7] R. Tamme, D. Laing, and W. D. Steinmann, "Advanced thermal energy storage technology for parabolic trough," *J. Sol. Energ.-T. ASME*, vol. 126, pp. 794–800, 2004.

[8] J. L. Shyu, R.J. and L. Fang, "Thermal analysis of stratified storage tanks," *J. Sol. Energ.-T. ASME*, vol. 111, pp. 54–61, 1989.

[9] I. Rodríguez, J. Castro, C. Pérez-Segarra, and A. Oliva, "Unsteady numerical simulation of the cooling process of vertical storage tanks under laminar natural convection," *Int. J. Therm. Sci.*, vol. 48, pp. 708–721, 2009.

[10] L. J. Shah and S. Furbo, “Entrance effects in solar storage tanks,” *Sol. Energy*, vol. 75, pp. 337–348, 2003.

[11] N. Calvet, J. C. Gomez, A. Faik, V. V. Roddatis, A. Meffre, G. C. Glatzmaier, S. Doppiu, and X. Py, “Compatibility of a post-industrial ceramic with nitrate molten salts for use as filler material in a thermocline storage system,” *Appl. Energ.*, vol. 109, pp. 387–393, 2013.

[12] H. Michels and R. Pitz-Paal, “Cascaded latent heat storage for parabolic trough solar power plants,” *Sol. Energy*, vol. 81, pp. 829–837, 2007.

[13] M. Liu, W. Saman, and F. Bruno, “Review on storage materials and thermal performance enhancement techniques for high temperature phase change thermal storage systems,” *Renew. Sust. Energ. Rev.*, vol. 16, pp. 2118–2132, 2012.

[14] H. Shabgard, C. W. Robak, T. L. Bergman, and A. Faghri, “Heat transfer and exergy analysis of cascaded latent heat storage with gravity-assisted heat pipes for concentrating solar power applications,” *Sol. Energy*, vol. 86, no. 3, pp. 816–830, 2012.

[15] K. Nithyanandam, R. Pitchumani, and A. Mathur, “Analysis of a latent thermocline storage system with encapsulated phase change materials for concentrating solar power,” *Appl. Energ.*, vol. 113, pp. 1446–1460, 2014.

[16] S. M. Flueckiger and S. V. Garimella, “Latent heat augmentation of thermocline energy storage for concentrating solar power —A system-level assessment,” *Appl. Energ.*, vol. 116, pp. 278–287, 2014.

[17] W. Steinmann and R. Tamme, “Latent heat storage for solar steam systems,” *J. Sol. Energ.-T. ASME*, vol. 130, pp. 011004–1–011004–5, 2008.

[18] P. Galione, C. D. Pérez-Segarra, I. Rodríguez, A. Oliva, and J. Rigola, “Multi-layered solid-PCM thermocline thermal storage concept for CSP plants. Numerical analysis and perspectives,” *Appl. Energ.*, vol. 142, pp. 337–351, 2015.

[19] P. Galione, C. D. Pérez-Segarra, I. Rodríguez, O. Lehmkuhl, and J. Rigola, “A new thermocline-pcm thermal storage concept for CSP plants. Numerical analysis and perspectives,” in *Proceedings of the SolarPACES 2013 International Conference*, vol. 49 of *Energy Procedia*, pp. 790–799, Elsevier, 2014.

[20] R. Damle, O. Lehmkuhl, G. Colomer, and I. Rodríguez, “Energy simulation of buildings with a modular object-oriented tool,” in *Proc. ISES Solar World Congress 2011*, 2011.

[21] N. Wakao, S. Kaguei, and T. Funazkri, "Effect of fluid dispersion coefficients on particle-to-fluid heat transfer coefficients in packed beds," *Chem. Eng. Sci.*, vol. 34, pp. 325–336, 1979.

[22] R. Krupiczka, "Analysis of thermal conductivity in granular materials," *Int. Chem. Eng.*, vol. 7, no. 1, pp. 122–144, 1967.

[23] A. Nakayama, F. Kuwahara, and Y. Kodama, "An equation for thermal dispersion flux transport and its mathematical modelling for heat and fluid flow in a porous medium," *J. Fluid Mech*, vol. 563, pp. 81–96, 2006.

[24] R. G. Holdich, *Fundamentals of particle technology.* Midland Information Technology and Publishing, 2002.

[25] N. Nallusamy, S. Sampath, and R. Velraj, "Experimental investigation on a combined sensible and latent heat storage system integrated with constant/varying (solar) heat sources," *Renew. Energ.*, vol. 32, pp. 1206–1227, 2007.

[26] I. Rodríguez, C. D. Pérez-Segarra, O. Lehmkuhl, and A. Oliva, "Modular object-oriented methodology for the resolution of molten salt storage tanks for CSP plants," *Appl. Energ.*, vol. 109, pp. 402–414, 2013.

[27] S. Torras, C. D. Pérez-Segarra, I. Rodríguez, J. Rigola, and A. Oliva, "Parametric study of two-tank TES systems for CSP plants," in *Proceedings of the SolarPACES 2014 International Conference*, 2014.

[28] U. Herrmann and R. Kistner, "The Andasol Project," tech. rep., FLABEG Solar Int. GmbH, Solar Millennium AG, 2002. Workshop on Thermal Storage for Trough Power Systems, `http://www.nrel.gov/csp/troughnet/pdfs/uh_anda_sol_ws030320.pdf`.

[29] A. B. Zavoico, "Solar power tower design basis document," Tech. Rep. SAND2001-2100, Sandia National Laboratories, 2001.

[30] C. Xu, Z. Wang, Y. He, X. Li, and F. Bai, "Sensitivity analysis of the numerical study on the thermal performance of a packed-bed molten salt thermocline thermal storage system," *Appl. Energ.*, vol. 92, pp. 65–75, 2012.

Multi-layered solid-PCM thermocline thermal storage for CSP. Numerical evaluation of its application in a 50MWe plant.

Short title: MLSPCM thermocline numerical evaluation for CSP

P.A. Galione[a,b], C.D. Pérez-Segarra[a,*], I. Rodríguez[a], S. Torras[a], J. Rigola[a]

[a] *Heat and Mass Transfer Technological Center (CTTC),Universitat Politècnica de Catalunya - BarcelonaTech, ETSEIAT, Colom 11, 08222, Terrassa (Barcelona), Spain*
[b] *Instituto de Ingeniería Mecánica y Producción Industrial (IIMPI), Universidad de la República (UdelaR), Uruguay*

Abstract

Thermocline storage concept is considered as a possible solution to reduce the cost of thermal storage in concentrated solar power (CSP) plants. Recently, a multi-layered solid-PCM (MLSPCM) concept —consisting of a thermocline-like tank combining layers of solid and phase change filler materials— has been proposed. This approach was observed to result in lower thermocline degradation throughout charge/discharge cycles, due to the thermal buffering effect of the PCM layers located at both ends of the tank. MLSPCM prototypes designed for a pilot scale plant were numerically tested and compared against other designs of single-tank thermocline systems, such as: solid-filled thermocline, tanks filled with a single encapsulated PCM and cascaded-PCM configurations. Results showed promising results of the MLSPCM configurations for their potential use in CSP plants.

In this work, the MLSPCM concept is used for designing a thermal energy storage (TES) system for a CSP plant with the dimensions and operating conditions of a parabolic trough plant of 50 MWe, similar to Andasol 1 (Granada, Spain). The performance evaluation of each of the proposed prototypes is virtually tested by means of a numerical methodology which considers the heat transfer and fluid dynamics phenomena present in these devices. Two sets of cases are considered, one with the objective of testing the TES systems individually, by defining specific operating conditions and taking the systems to a periodic steady state; and another, aiming to evaluate their performance after several days of operation in a CSP plant, in which the weather variability and the thermal behavior of the tank walls and foundation are simulated. Thermal performance parameters, such as total energy and exergy stored/released and the efficiency in the use of the storage capacity, are calculated and compared with those obtained by other thermocline-like configurations (single-solid and single-PCM), and with a reference 2-tank molten-salt system. Obtained results allow to continue considering the

*Corresponding author
Email addresses: pedrog@cttc.upc.edu, pgalione@fing.edu.uy (P.A. Galione), cttc@cttc.upc.edu (C.D. Pérez-Segarra)

MLSPCM concept as an interesting alternative for thermal storage in CSP facilities.

Keywords: Thermal Energy Storage, CSP, Phase Change Materials, Thermocline, Multi-Layered Solid-PCM, Numerical Analysis

NOMENCLATURE

A	Surface area
A_t	Transversal area of tank
A_w	Internal surface area of tank's lateral wall
C_p	Specific heat at constant pressure
d_p	Diameter of filler PCM capsule/solid particle
ex	Exergy
f	Mass liquid fraction (PCM)
F	Capsule volume fraction filled by PCM
g	Gravity acceleration
h	Specific total enthalpy
h_{conv}	Convection coefficient
k	Thermal conductivity
k_{eff}	Effective thermal conductivity
L	Specific latent enthalpy
$m, \dot{m}$	Mass and mass flux
N_r	Number of control volumes of one filler particle/capsule
N_x	Number of tank sections
p	Pressure
$\dot{Q}$	Thermal power
r	Radial direction
R_{cond}	Thermal conduction resistance of capsule shell
R_{conv}	Convection resistance between fluid and capsule/solid filler
t	Time
T	Temperature
U_{TC-Sh}	Heat transfer convection coefficient between the fluid in the packed bed and the tank shell
v	Velocity (seepage velocity in packed beds)
V	Volume
Δt	Time step
Δx	Tank section height
ϵ	Volume liquid fraction (porosity)
η	Efficiency
μ	Dynamic viscosity
ρ	Density

Superscripts and subscripts:

f	Fluid flow
fm	Filler material (PCM or solid)
i	Index of tank section/control volume
$i \pm 1/2$	Index of tank section's face limiting i and $i \pm 1$
in	Tank inlet
j	Index of capsule/solid filler control volume
$j \pm 1/2$	Index of filler control volume's face limiting j and $j \pm 1$
l, liq	Liquid phase
nom	Nominal
out	Tank outlet
s, sol	Solid phase

Abbreviations:

CFL	Courant, Friedrich, Lewy condition
CSP	Concentrated Solar Power
DNI	Direct Normal Irradiation
HTF	Heat Transfer Fluid
MLSPCM	Multi-Layered Solid-PCM
PB	Power Block
PCM	Phase Change Material
SF	Solar Field
TES	Thermal Energy Storage

1. Introduction

Thermal energy storage (TES) allows a more effective use of solar energy by reducing the mismatch between the energy supply and its demand. In concentrated solar power (CSP) facilities, TES systems increase the reliability and generation capacity of the whole system and reduce the levelized cost of electricity [1, 2].

Nowadays, many CSP plants incorporate a molten-salt two-tank TES system (e.g. Andasol and Extresol in Spain, Crescent Dunes and Solana in USA), which makes use of the sensible energy capacity of the molten-salt [3, 4]. However, different TES designs resulting in lower investment costs are currently under study, some of which are also based on the sensible energy capacity of the materials, such as thermocline single-tanks [5, 6] and concrete storage designs [7].

In thermocline systems, both high and low temperature fluids are contained in the same tank. Thermal stratification is the mechanism separating them, and the thermal gradient produced within the fluid is called thermocline. The thermocline thickness indicates the amount of thermal mixing, which may be due to natural convection effects (see e.g. [8, 9]) and strong inlet flow currents [10], and is intended to be maintained at a minimum. A modification to the original concept, aiming at reducing the thermal mixing and also reducing the amount of molten-salt used, is to fill the tank with a cheaper solid material such as quartzite rocks, granite, sand [5], asbestos-containing wastes [11], forming a porous packed bed through which the heat transfer fluid flows.

On the other hand, several researchers have been investigating the use of phase change materials (PCM) as thermal storage media, taking advantage of the high energy density present in the phase-change phenomena. For example, Michels and Pitz-Paal [12] performed a numerical and experimental investigation of storage systems using different PCMs with cascaded melting points, contained in shell and tube heat exchangers, for parabolic trough CSP plants. Liu et al. [13] carried out an extensive review of high-temperature phase change storage materials and of thermal enhancement techniques. Shabgard et al. [14] performed a numerical analysis of cascaded latent heat storage with gravity-assisted heat pipes for CSP applications. Nithyanandam et al. [15] studied packed bed thermal storage with encapsulated PCMs for CSP by means of a numerical model. They performed parametric analyses and established guidelines for the design of latent storage systems. Flueckiger et al. [16] analyzed latent-heat-augmented thermocline storage for CSP using an integrated system-level model for the whole CSP plant and evaluated the effect of the increase of the storage capacity with the latent heat. Limitations in the thermal performance of tanks including PCMs were observed, while some improvement was obtained with some of the cascaded PCM designs.

Furthermore, Steinmann and Tamme [17] studied the combination of latent and sensible storage heat exchangers specially suited for direct steam generation solar field technology (DSG). A PCM storage unit was intended for producing the vapor generation (evaporation) and two concrete storage units for storing the sensible portion of the fluid's energy (pre and superheating).

In previous works [18, 19], a new concept of thermocline-like thermal storage device named multi-layered solid-PCM (MLSPCM), consisting of a packed bed of different layers of solid and PCM filler materials, was presented. There, MLSPCM designs of the same dimensions and operating conditions as those of the pilot scale tank presented by Pacheco et al. [5], were numerically tested and compared against other designs of single-tank thermocline-like systems such as: single-solid, single-PCM and cascaded-PCM filler configurations. Results obtained for MLSPCM prototypes showed to be promising for their potential use in CSP plants.

In this work, the MLSPCM concept is used for making up a TES system for a CSP plant. A parabolic trough of 50MW of electric output is assumed, similar to Andasol 1 plant (Granada, Spain). With this aim, two levels of analysis are carried out. Firstly, numerical simulations similar to those presented in [18] are carried out, in order to evaluate the performance of the full-scale TES prototypes under specific conditions. In these, the TES is charged and discharged consecutively until reaching a periodic steady state. Secondly, in order to test the different TES systems under operating conditions closer to those of a CSP facility, another analysis is performed incorporating weather variation, idle processes and thermal losses to the tank shell and foundation, for several days of plant operation. For this, a modular object-oriented code is used [20], which links the different models corresponding to the elements under study.

Similarly as in the pilot-scale prototypes presented in [18, 19], some full-scale MLSPCM configurations are observed to produce an increase of the efficiency in the use of total capacity when compared with other thermocline-like designs, especially in the isolated TES analysis. Although consideration of the variability of the operating conditions results in closer values of accumulated energy and efficiency, MLSPCM concept continues to present advantages over the solid-filled thermocline design. The advantages against single-PCM packed beds are more clear, since a similar storage is obtained using a much lower amount of encapsulated PCM, which is assumed to be a costly component compared to the solid filler material. As a result of the study, a MLSPCM prototype considered equivalent to the reference 2-tank system is presented, resulting in the same amounts of energy and exergy delivered to the power block in both analyses.

1.1. MLSPCM concept

Figure 1 shows a sketch of a three-layered MLSPCM TES tank. It consists of a tank containing a porous bed through which a fluid passes delivering/absorbing energy to/from the filler material, as in a "conventional" thermocline tank. However, the MLSPCM concept uses a combination of layers of different filler materials, with one solid and at least one containing PCM. The PCM layers are placed in the extremes of the tank, and their melting points are chosen to be within the admissible temperature ranges for the fluid coming out of the tank through the outlet located close to the PCM filler. These ranges are determined by the HTF temperature required by the solar receivers (in the TES charging process) and the power block (in the TES discharge), which impose temperature thresholds to HTF inflow, for their proper operation.

In a MLSPCM with three layers, as that shown in Figure 1, the PCM located at the top is chosen to have a high melting point (within the admissible range of temperatures for the fluid coming out in the discharge process), and the one located at the bottom is chosen with a low melting point (within the range admitted for the outflow in the charge process).

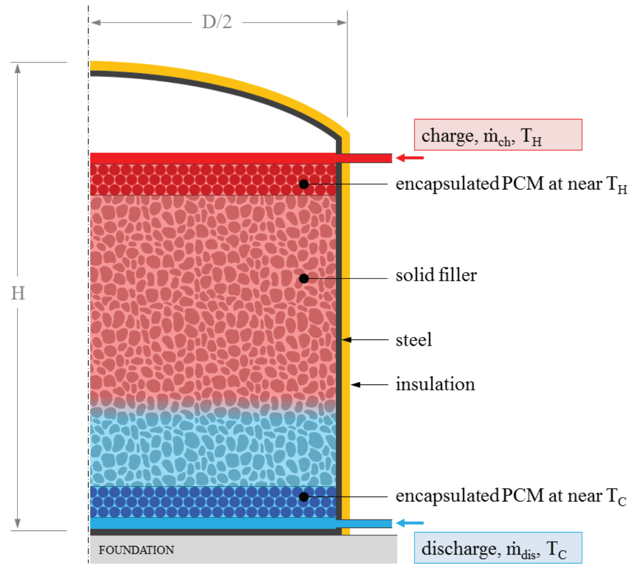

Figure 1: Sketch of a MLSPCM TES tank with three layers

The PCM layers not only increase the total storage capacity of the TES tank (with respect to a single-solid filled tank), but also act as thermal "buffers" by keeping the outflow temperatures within the admissible temperature ranges. Therefore, there is an increase in the operating time (since the processes can continue while the outflow temperatures remain within these ranges), and thus in the amount of energy which can be effectively stored/withdrawn, resulting in a high efficiency in the use of the total (ideal) storage capacity.

2. Mathematical modeling and numerical implementation

The thermocline-like TES considered are formed by different elements: thermocline packed bed (filler material and HTF), tank foundation and tank walls, which interact with each other through their boundary conditions. This implementation has been performed within the NEST platform [20], which allows linking between different elements of the thermal system. The mathematical model considers the transient behavior of the thermocline-like packed beds, the tank walls and insulation, taking into account the variable outdoor conditions (DNI, ambient temperature). A brief mathematical description, focused on the modeling of the packed bed, is presented hereafter.

2.1. Packed bed

The model presented in [18] is used. Mass, momentum and energy conservation equations have to be solved in order to be able to simulate the thermal behavior of a thermocline-like tank. One-dimensionality in the fluid flow and in the heat transfer inside particles/capsules is assumed. Natural

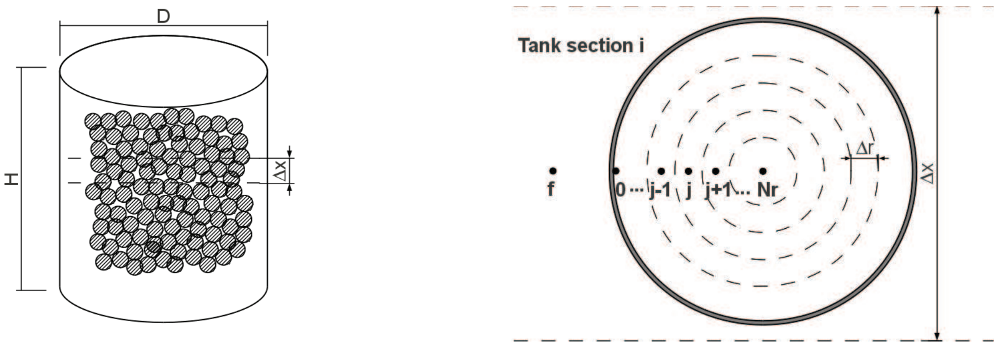

(a) Sketch representing the cylindrical container with the PCM capsules packed in a random fashion

(b) discretization details of the tank and of a representative particle/capsule, indicating the sub-indices used for tank sections (i) and capsule control volumes (j)

Figure 2: Domain and discretization.

convection and contact melting inside PCM capsules is neglected, as well as thermal conduction between different particles/capsules.

In the filler particles/capsules, a radial variation of the temperature is assumed. Conservation equations are discretized using the Finite Volume Method (FVM). The tank is divided in N_x transversal cylindrical sections of height Δx (see Fig. 2a). In each tank section, a single representative particle/capsule needs to be simulated, due to the one-dimensionality assumption. This filler particle/capsule is discretized in the radial direction in N_r control volumes, as shown in Fig. 2b.

For the heat transfer fluid (HTF) going through the porous bed, the semi-discrete energy conservation equation of the fluid in the i$^{\text{th}}$ tank section ($i = 1...N_x$) results in:

$$\rho_f \epsilon_i V_i C_{p,f} \frac{\partial T_{i,f}}{\partial t} = A_t \left(k_{eff} \frac{\partial T_f}{\partial x} \right) \Bigg|_{i-1/2}^{i+1/2} - \dot{m} C_{p,f} (T_{i+1/2,f} - T_{i-1/2,f})$$
$$- n_{fm,i} \frac{T_{i,f} - T_{i,0}}{R_{conv,i} + R_{cond,i}} - U_{TC-Sh} A_{w,i} (T_{i,f} - T_{i,Sh}) \qquad (1)$$

where $T_{i,0}$ is the temperature of the internal surface of the particles/capsules (boundary node in fig. 2b). In the advective term (second in the right hand side) the fluid is assumed to be coming from section $i-1$ and going to section $i+1$.

R_{cond} stands for the thermal resistance in the PCM capsules due to the capsule shell. The mass of the shell is disregarded here and is not considered to add any thermal inertia. The calculation of the thermal resistance due to convection between the HTF and the filler material (R_{conv}) requires the fluid-to-bed Nusselt number, which is calculated using the correlation obtained from [21]:

The effective thermal conductivity (accounting for solid-phase conduction and thermal dispersion) is evaluated as the sum of stagnant and dispersion effective conductivities, calculated with the correlations obtained from [22] and [23].

The energy balance for the inner nodes ($j = 1...N_r$) of the filler material (either PCM capsules or solid particles) remains:

$$\rho_{fm} F_i V_{i,j} \frac{\partial h_{i,j}}{\partial t} = \left(k_{fm} A \frac{\partial T}{\partial r} \right)_{i,j-1/2} - \left(k_{fm} A \frac{\partial T}{\partial r} \right)_{i,j+1/2} \tag{2a}$$

while for the boundary node ($j = 0$), in contact with the heat transfer fluid, results in:

$$\rho_{fm} F_i V_{i,0} \frac{\partial h_{i,0}}{\partial t} = \frac{T_{f,i} - T_{i,0}}{R_{conv,i} + R_{cond,i}} - \left(k_{fm} A \frac{\partial T}{\partial r} \right)_{i,1/2} \tag{2b}$$

where F_i indicates the volume fraction of the capsules occupied by the PCM (F_i=1 for the solid particles). This value is between 0 and 1 and takes into account that a void space is needed in order to allow for the thermal expansion in the melting.

The relations between enthalpy and temperature for the filler materials (solid and/or PCM) are:

$$\begin{aligned}
&h - h_0 = C_{p,s}(T - T_0), && T \leq T_s \\
&h - h_0 = C_{p,s}(T - T_0) + fL, && T_s < T \leq T_{sl} \\
&h - h_0 = C_{p,l}(T - T_{sl}) + C_{p,s}(T_{sl} - T_0) + fL, && T_{sl} < T \leq T_l \\
&h - h_0 = C_{p,l}(T - T_{sl}) + C_{p,s}(T_{sl} - T_0) + L, && T_l < T
\end{aligned}$$

where T_{sl} indicates the temperature in the phase change range chosen as the transition temperature for the specific energy from solid to liquid, or vice versa. Mass liquid fraction (f) ranges from 0 (pure solid) to 1 (pure liquid) and is calculated as a linear function of temperature in the phase change interval:

$$f = \frac{T - T_s}{T_l - T_s} \tag{3}$$

By taking a very narrow temperature range ($T_l - T_s$), fixed melting point PCMs can also be modeled with this approach. Hence, a unique value of h exists for each value of T, and the energy balance (Eq. (2)) is expressed with T as the only variable.

For evaluating the power generating potential of the energy delivered by the thermal storage, the exergy global balance of the heat transfer fluid is calculated in the following manner:

$$\dot{m}(ex_{out} - ex_{in}) = \dot{m} C_{p,f} (T_{out} - T_{in} - T_{ref}\, ln \frac{T_{out}}{T_{in}}) \tag{4}$$

where T_{ref} is the temperature corresponding to the dead state, which in this work has been taken as 45℃ due to being a reasonable value for the temperature at which the vapor is condensed in the power generation block.

To determine the pressure drop in the packed bed, the Carman correlation is used [24]:

$$\left.\frac{\delta p}{\delta x}\right|_i = \pm\left(\frac{5}{Re_{1,i}} + \frac{0.4}{Re_{1,i}^{0.1}}\right)\frac{6\rho_f v_f^2(1-\epsilon_i)}{d_{p,i}\epsilon_i^3} - \rho_f g \tag{5}$$

$$\text{where } Re_{1,i} = \frac{\rho_f v_f d_{p,i}}{6(1-\epsilon_i)\mu_f} \text{ (spherical particles) and } v_f = \frac{\dot{m}}{\rho_f A_t}$$

In this equation x increases from the bottom to the top, and therefore, the positive sign is used in the discharge of the tank while in the charge process the negative sign is used. The last term accounts for the pressure reduction/increase due to the gravitational action.

For further details of the model used, please refer to reference [18].

2.1.1. Discretization and validation

The diffusive term of Eq. (1) has been discretized using a 2$^{\text{nd}}$ order central difference spatial and a fully implicit temporal integration schemes. The convective term is time-integrated using a fully explicit, 1$^{\text{st}}$ order scheme; and depending on the Péclet number ($\Delta x\, v_f/k_{eff}$), it is discretized either using an upwind scheme (coarser meshes) or a centered scheme (finer meshes), avoiding unboundedness problems on the one side and high numerical diffusion on the other.

The criterion for choosing the time step is similar to that indicated in [18]. If the convective term of the energy equation of the HTF is of higher strength than the diffusive term, a CFL number of 1 is imposed ($\Delta t = \epsilon\Delta x/v_f$). However, if the diffusive term is stronger, the time step is determined by imposing $\Delta t_{diff} = \mathrm{C}(\epsilon\rho C_p\Delta x^2/2k_{eff})$ (where C is chosen between 0.5 and 1) for accuracy reasons. It should be noted that for the cases studied within this work, the time steps resulting from this last condition are similar to those obtained by the CFL=1 condition with the tanks operating under the nominal mass flux.

Therefore, when the mesh is coarse enough, the upwind scheme is used for the convective term and the time step is determined by setting CFL = 1. On the other hand, when the grid is fine enough, the diffusive term results in a comparable or (higher) strength than the convective term, in which case, the centered scheme is used and the CFL number is set to be lower than 1. For further details on the discretization procedure please refer to [18].

The validation of the model was performed against two experimental cases, one of a thermocline tank filled with a mixture of Quartzite rock and sand (experimental work of Pacheco et al. [5]) and another of a packed bed of encapsulated PCM (experimental work of Nallusamy et al. [25]). The results of both validation cases are presented in [18]; where a very good agreement was obtained for the first case and also for the HTF temperature profiles of the second case, and some differences with the PCM temperature profiles of the latter were observed. These discrepancies have been attributed to several reasons, such as the model not accounting for the natural convection and contact melting phenomena inside the PCM capsules, and also to uncertainties in the thermo-physical properties of the PCM and in the position of the thermocouples inside the capsules in the experimental setup. In overall, a good agreement has been obtained for the purposes of this work.

2.2. Tank walls, insulation and foundation

The models used for simulating the heat transfer through the tank walls, insulation and foundation are those presented in [26, 27]. A transient 1D heat balance is performed to find the temperature of the tank walls and the insulation in each tank section. For the foundation, a simplified zonal 1D model has been used. More details about the formulation used for these components can be found in references [26, 27].

2.3. Linking the different components

The connection between the different parts of the system (packed bed + HTF, tank walls + insulation, foundation and outdoor conditions; see Figure 1) is performed by the NEST code. This code is a modular object-oriented tool which connects the different models of the different objects through their boundary conditions, allowing independent solution methods for each object (besides their boundary connections). Furthermore, the NEST platform has been designed to work in a parallel computing infrastructure, allowing faster resolution of complex problems.

The resolution algorithm for the cases presented herein is of the Jacobi kind, where each element uses the boundary conditions passed by the connected elements in the previous iteration.

For more insight on the NEST platform, the reader is referred to [20, 26].

3. Cases of isolated TES under nominal conditions

Two levels of analysis are carried out in this work. The first one is developed in this section, consisting in an isolated analysis of the different TES configurations, under specific operating conditions. Therefore, flow inlet conditions are constant (and equal) for both charge and discharge processes, and no thermal losses to the ambient (nor to the walls and foundation) are considered. Thermal performance is evaluated after reaching a periodic state, which is achieved when consecutive charge/discharge cycles result in the same stored/released energy. With this, thermal performance is independent of the initial state of the first charge/discharge cycle.

Different configurations of thermocline tanks are considered by changing the filler material used. Single-solid, single-PCM and MLSPCM configurations are tested and compared against the ideal performance (no thermal losses) of the two-tank system considered as a reference. The dimensions of one tank of the two-tank molten-salt reference system are 13m height by 38m diameter (adopted from those of Andasol 1 facility [28]). Single-tank systems will be firstly designed with these same dimensions, and finally the diameter will be increased for one selected MLSPCM configuration in order to achieve the same thermal storage in the periodic state as with the molten salt system.

TES charge and discharge processes are carried out with molten salt at 390℃ and 290℃, entering through the inlets placed at its top and bottom, respectively. A mass flow of 948 kg/s is assumed, which is the nominal value for Andasol 1 plant [28].

Furthermore, the following operating conditions are assumed:

- Operating time is not fixed but depends on the temperature of the fluid coming out of the tank at each process. Temperature thresholds are imposed to avoid outlet temperatures too cold or too hot to be sent to the receiving equipment (i.e solar field and power block). The temperature ranges between the thresholds and the highest (discharge) or lowest (charge) will be referred to as "admissible" temperature ranges. Each process is stopped when the temperature of the fluid coming out of the tank goes out from these admissible ranges.

  Here, both ranges have been assumed to be 15% of the maximum temperature interval (100℃); i.e. 290-305℃ for the charging process and 375-390℃ for the discharge.

- Ambient losses are neglected [$U_{TC-Sh} = 0$ in Eq. (1)].

- Several consecutive charge/discharge cycles are simulated until a periodic thermal state is reached, i.e. when there is negligible variation of the stored/released energy between consecutive cycles. Since ambient losses are neglected, the same energy that is stored in the charge must be released in the discharge at the periodic state.

Since the admissible temperature intervals for both charge and discharge processes are quite narrow, outlet fluid temperatures for all the cases are very similar. Therefore, a higher operation time is directly related to a higher stored (or released) energy.

In Table 1, a code for each prototype/configuration is defined. The thermocline-like prototypes can be classified according to the filler material/s used as: single-solid (A); single-PCM (B) and multi-layered solid-PCM (C). Percentages between brackets indicate the portion of total height occupied by each filler material. It should be noted that the chosen PCMs are fictitious, having the same thermal properties as those of potassium hydroxide (KOH) but with different fusion temperatures.

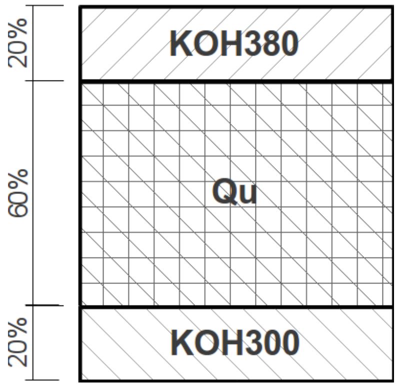

Figure 3: Sketch of MLSPCM prototype C1.

The exception is case B1, where KOH is considered with its actual melting point (360℃ according to [12]). This procedure has been adopted in order to account for the variations in performance exclusively due to the change in the fusion temperature of the PCMs. Figure 3 depicts a sketch of one of the prototypes tested. Table 2 shows the physical properties used in the simulations. The solid filler material adopted here is a mixture of quartzite rock and sand [5]. For the filler material, both PCM and solid, a diameter of 15mm is adopted. Porosity is 0.4 for the PCM layers and 0.22 for the packed bed of quartzite rock and sand. The volume fraction of capsules occupied by PCM is 85%.

Table 1: Codification of prototypes.

Filler material/s[1] - Tank dimensions	Code
2-Tank molten salt - 13m×38m	2-TANK
Quartzite rock & sand (Qu) (100%) - 13m×38m	A1
KOH (100%) - 13m×38m	B1
KOH380 (100%) - 13m×38m	B2
KOH300 (100%) - 13m×38m	B3
MLSPCM: KOH380-Qu-KOH300 (20%-60%-20%) - 13m×38m	C1
MLSPCM: KOH380-Qu-KOH300 (5%-90%-5%) - 13m×38m	C2
MLSPCM: KOH380-Qu-KOH300 (5%-90%-5%) - 13m×43.7m	C3
Quartzite rock & sand (Qu) (100%) - 13m×43.7m	A2

[a]Materials KOHXXX (where XXX is a 3 digit number) are fictitious PCMs with fusion temperatures indicated by the number XXX (e.g. 300℃), whose thermal properties are equal to those of KOH (whose fusion temperature is 360℃). The order in which the materials are indicated is the one in which they are placed inside the tank, from the top to the bottom. Between brackets, the proportion of the tank height occupied by each filler layer is indicated.

Table 3 shows the mass of solid filler material, PCM and HTF contained for each prototype. Due

Table 2: Thermo-physical properties

	Quartzite rock & sand [30]	PCM [12]	Molten Salt [29]
ρ $[kg/m^3]$	2500	2040	1873.8
$C_{p,s}$ $[J/kg\,K]$	830	1340	-
$C_{p,l}$ $[J/kg\,K]$	-	1340	1501.5
k_s $[W/m\,K]$	5.69	0.5	-
k_l $[W/m\,K]$	-	0.5	$0.443 + 1.9 \times 10^{-4} T(^{\text{o}}\text{C})$
μ $[Pa\,s]$	-	-	$22.714 \times 10^{-3} - 0.12 \times 10^{-3} T + 2.281 \times 10^{-7} T^2 - 1.474 \times 10^{-10} T^3$
L $[J/kg]$	-	1.34×10^5	-

to the higher porosity of the PCM layers, the configurations including encapsulated PCMs have a higher amount of confined heat transfer fluid. Furthermore, as the solid filler material is more dense than the PCM, a higher amount of the former results in a higher total mass. The same table also presents data of the storage capacity for each configuration, i.e. the maximum amount of energy that could (theoretically) be stored taking into account both sensible and latent energy contributions, with a temperature jump of 100℃ (290℃- 390℃). In the case of the 2-tank system, the stored energy at the periodic state is equal to the capacity, since this system is not affected by the phenomenon of thermocline degradation and the thermal losses to the ambient are not considered in this part of the study.

3.1. Results and discussion

Table 4 shows the quantitative results obtained from the simulation of the different cases considered, after the periodic steady state has been reached. The different cases (or prototypes) are divided into two groups, one in which the tank dimensions are the same as those of the 2-tank system, and another in which the diameter of the tank is increased.

Results depicted in Table 4 correspond to simulations run with a grid with $N_x = 1040$ and $N_r = 10$. These have been checked to be good in terms of grid independence, since comparing against results obtained with a grid with double resolution (for some cases), the differences in the values of stored energy were lower than 0.6%.

Table 3: Mass confined inside the tank and storage capacity

Mass data (ton)	2-TANK	A1	B1	B2	B3	C1	C2	C3	A2
Mass of PCM	0.0	0.0	13013.4	13013.4	13013.4	5205.4	1301.3	1721.0	0.0
Mass of solid filler material	0.0	28749.8	0.0	0.0	0.0	17249.9	25874.8	34219.5	38021.6
Mass of confined HTF	27629.3	6078.4	11051.7	11051.7	11051.7	8067.8	6575.8	8696.5	8038.7
Total mass	27629.3	34828.3	24065.2	24065.2	24065.2	30523.0	33752.0	44637.0	46060.4
Storage Capacity									
Filler material (MWh)	0.00	662.84	968.78	968.78	968.78	785.22	693.44	917.07	876.61
Confined HTF (MWh)	1152.36	253.52	460.94	460.94	460.94	336.49	274.26	362.71	335.28
Total (filler+HTF) (MWh)	1152.36	916.36	1429.72	1429.72	1429.72	1121.71	967.70	1279.78	1211.89
Total sensible energy (%)	100.0	100.0	66.1	66.1	66.1	82.7	95.0	95.0	100.0
Total latent energy (%)	0.0	0.0	33.9	33.9	33.9	17.3	5.0	5.0	0.0

3.1.1. Prototypes with tank dimensions of 13m × 38m

Cases A1 to C2 correspond to different thermocline configurations of tanks with the same dimensions as that of a single tank of the 2-tank system (13m × 38m).

As seen in previous works [18, 19], the single-solid-filled thermocline tank shows a degradation of the thermocline throughout consecutive charge/discharge cycles, due to the restrictions on the outlet fluid temperature. As a result, the stored energy at the periodic state is around 80% of its storage capacity. This value is higher than that obtained for the small scale prototype tested in [18] (with dimensions of 5.2m × 3m), where a utilization of around 63% of the capacity was obtained. The reason for this is that the thermocline height in both cases is similar —around 2m in the case of [18] and 3m in the present case (see fig. 4)—while the height of the tank is very different, resulting in a lower thermocline zone relative to the height for the case presented here ($\sim$ 23% vs. $\sim$ 33.3%).

Table 4: Performance results for each configuration

	Diameter = 38m							Diameter = 43.7m	
Results	2-tank	A1	B1	B2	B3	C1	C2	C3	A2
Operation time (h)[1]	8.10	5.18	3.06	6.61	6.61	7.12	6.43	8.54	6.88
Stored Energy in Filler material (MWh)	0.0	529.7	226.6	501.6	501.5	659.2	645.8	857.7	703.4
Stored Energy (Filler + confined HTF) (MWh)	1152.4	732.7	432.4	902.6	902.5	937.6	894.6	1188.7	972.9
Stored Energy / Storage capacity (%)	100.0	80.0	30.2	63.1	63.1	83.6	92.4	92.9	80.3
Stored Energy / Stored Energy in 2-tank (%)	100.0	63.6	37.5	78.3	78.3	81.4	77.6	103.2	84.4
Sensible energy stored / Total stored (%)	100.0	100.0	97.4	90.9	90.9	80.5	94.8	94.8	100.0
Latent energy stored / Total stored (%)	0.0	0.0	2.6	9.1	9.1	19.5	5.2	5.2	0.0
Effective mass of PCM changing phase (%)	-	-	2.3	16.9	16.9	94.3	95.3	96.0	0.0
Exergy difference at charge (MWh)	-553.2	-352.0	-207.7	-433.4	-436.2	-453.2	-430.3	571.8	-467.4
Exergy difference at discharge (MWh)	553.2	351.6	207.3	430.54	433.3	447.3	428.7	569.7	466.8
Exergy at discharge / Exergy at discharge of 2-tank (%)	100.0	63.5	37.5	77.8	78.3	80.9	77.5	103.0	84.4
Pumping energy / Stored Energy (%)	0.08	0.09	0.09	0.09	0.09	0.09	0.09	0.09	0.09

[a] In cases where the charge and discharge operation times are different, (e.g. B2 and B3) the mean value between processes is shown.

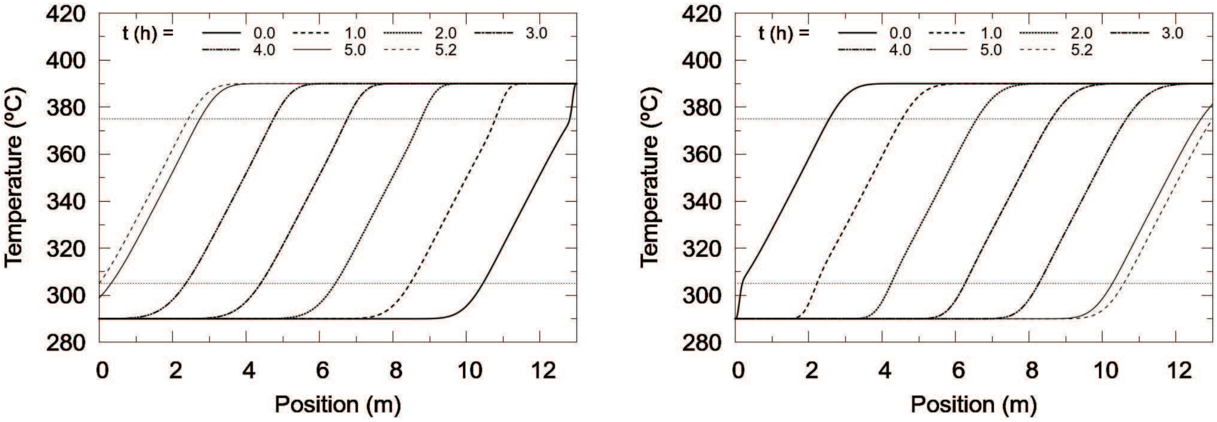

(a) Charge **(b)** Discharge

Figure 4: Case A1. Periodic state. Temperature maps at various instants. The chronological order of the curves is from right to left for the charge process and from left to right for the discharge. Horizontal dotted lines indicate the threshold temperatures.

Case A1 results in both delivered energy and exergy to the PB of ∼64% with respect to the obtained with the 2-tank system.

Prototype of case B1 is filled with a single encapsulated PCM with a fusion temperature of 360℃ (KOH) which is outside both admissible temperature ranges for the outgoing fluid. The thermal performance of the prototype filled with this encapsulated PCM is the worst of all the cases studied.

The percentage of PCM effectively changing phase between processes is very low (2.3%) and also the usage of the storage capacity (30%).

Figure 5 shows the temperature maps for the periodic state. It can be observed that the area between the initial and last temperature curves is very small, resulting in a very low utilization of the sensible energy capacity of the system.

As observed in [18], the reason for this poor performance is that the melting point is not within any of both admissible temperature ranges. In the charging phase, the phase-changing zone (at 360℃) advances from the top of the tank to the bottom. Beyond this zone, both the fluid and filler materials are at a lower temperature, and thus, no melting of the PCM is occurring. At the begining of the charge, the temperature of the outflow is 290℃ but starts increasing after a while, when the hotter upstream fluid gets to the outlet. This continues until the threshold of 305℃is reached, when the charging process stops. At this point, a high portion of the PCM is at temperatures lower than the melting point (between 305-360℃), and therefore, has not absorbed energy in the form of latent heat. This portion of PCM (close to the bottom of the tank) is not able to release latent heat to the HTF in the subsequent discharge; where moreover, the PCM closer to the top is not able to solidify due to being at a temperature range between 360-375°C, at the end of the process. Therefore, at the periodic equilibrium state, only a small portion near the middle zone of the tank effectively changes phase from one process to the next, resulting in a very low utilization of the latent heat capacity of the PCM. Furthermore, the sensible capacity is also very poorly used, due to the limitation imposed by the phase-changing PCM to the range of temperatures allowed to the materials contained at both sides of it (between 290-360°C for the cold zone and between 360-390°C for the hot zone).

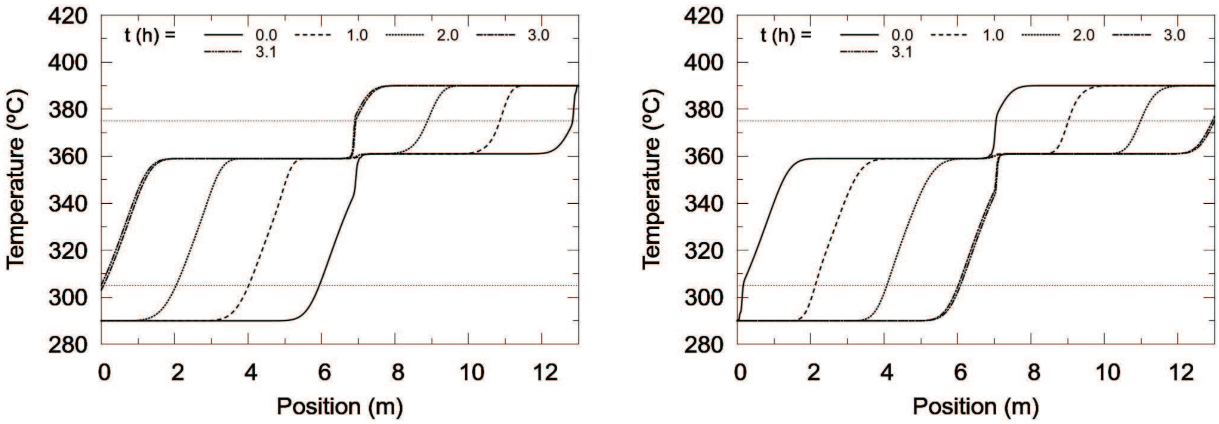

(a) Charge

(b) Discharge

Figure 5: Case B1. Periodic state. Temperature maps at various instants. The chronological order of the curves is from right to left for the charge process and from left to right for the discharge. Horizontal dotted lines indicate the threshold temperatures.

Cases B2 and B3 have the common feature of using PCMs whose melting points lie inside each of the admissible temperature ranges. Temperature maps for the periodic state of both cases are shown in figures 6 and 7. A first observation is that the area between the initial and final maps for both cases is significantly higher than that of case B1. As a result, a higher utilization of the storage capacity, and thus, a higher stored energy, is obtained with these prototypes. Due to the symmetry between key temperatures of cases B2 and B3 (melting points, thresholds and operating range), the resulting temperature maps for the periodic state are also symmetric and the thermal performance results for both cases are almost identical. It can be observed that the efficiency in the use of the phase change material and of the whole storage capacity are much higher than that of prototype B1, but not yet ideal (17% and 63%, respectively, for both B2 and B3). In these cases, the PCM located close to the outlet corresponding to the process whose admissible range contains the melting point (the one in the top for case B2 and the one in the bottom for case B3), act as a thermal buffers by not allowing the outflow temperature to escape from the admissible range, until it has changed phase. In the subsequent process, this portion changes phase again, since it is the first to encounter the cold/hot fluid coming through the inlet. Therefore, a higher portion of PCM effectively changes phase in the periodic state, also allowing a higher use of the sensible energy capacity of the PCM which does not melt/solidify.

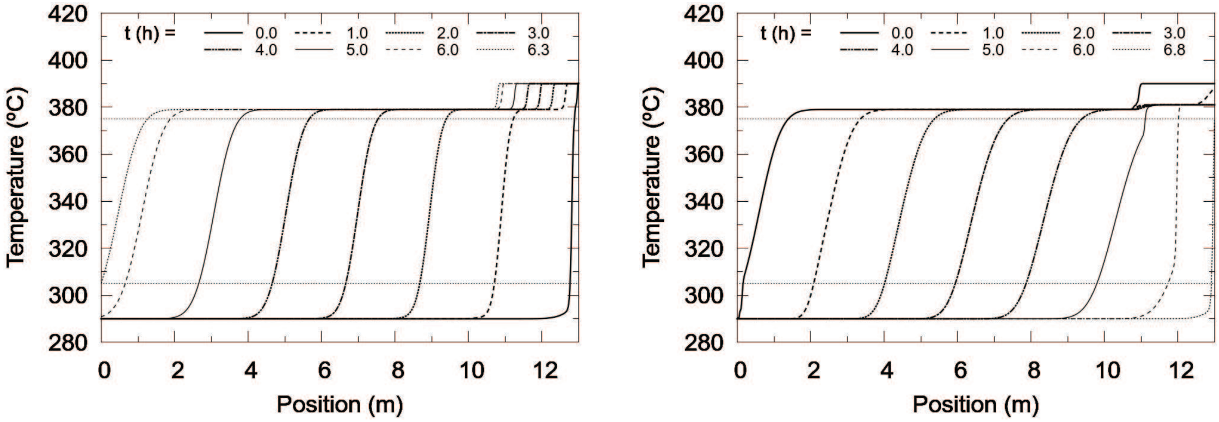

(a) Charge **(b)** Discharge

Figure 6: Case B2. Periodic state. Temperature maps at various instants. The chronological order of the curves is from right to left for the charge process and from left to right for the discharge. Horizontal dotted lines indicate the threshold temperatures.

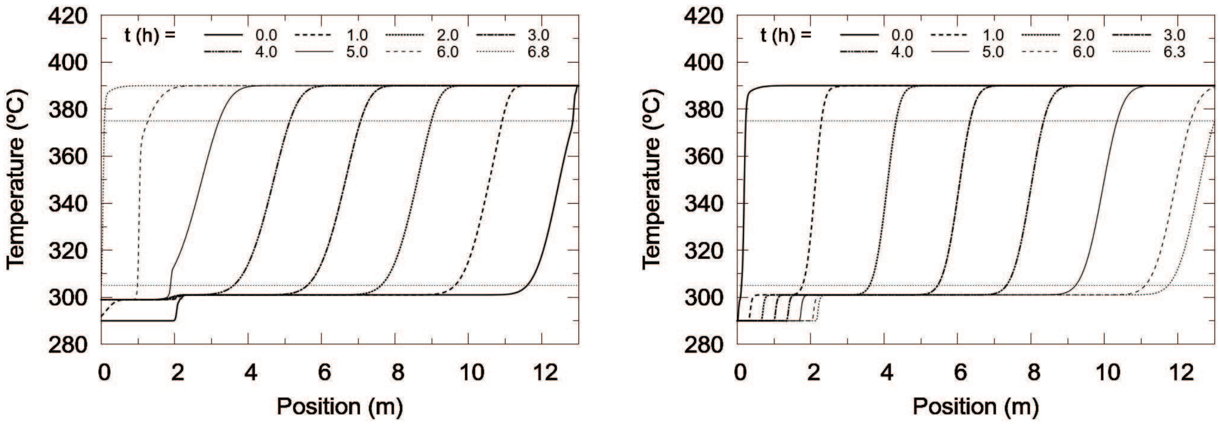

(a) Charge **(b)** Discharge

Figure 7: Case B3. Periodic state. Temperature maps at various instants. The chronological order of the curves is from right to left for the charge process and from left to right for the discharge. Horizontal dotted lines indicate the threshold temperatures.

Cases C1 and C2 are MLSPCM configurations with only two different PCMs collocated at both extremes of the tank and a solid filler material (quartzite rocks & sand) in the middle zone, forming a 3-layer arrangement, only differing in the width of the layers. Figure 3 shows a sketch of the configuration of prototype C1. Due to the symmetry of the operating conditions, the design of the filler materials configuration is also symmetric. The PCMs used are those whose melting points are contained in the admissible temperature ranges for the outgoing fluid in both processes, KOH380 and KOH300.

In [18], it was observed that only the energy contained in the HTF between the inlet temperature and the melting point of the PCM located at the inlet can be "used" for producing the phase-change of the PCM, at most. This is, in the charge process, only the energy contained between 390℃ (inlet) and 380℃ is available for melting the PCM layer of KOH380 (located at the top). Therefore, as only 10-12% of the whole energy available to be stored can be used for producing the phase-change of each PCM layer, then only 20-24% of the energy can be stored/released in the form of latent energy. Hence, in order to assure that most of the PCM will effectively undergo a change of phase, configurations with a latent energy capacity of less than 20% are considered here. Observe, from Table 3, that prototype C1 has a latent energy capacity of 17% of the total storage capacity and this value is only 5% in C2.

Performance results of these two cases, are the best in terms of efficiency in the use of the storage capacity (C1 84%, C2 92%) and in the use of the latent energy (94-95% of the PCM changing phase between processes). In terms of total energy and exergy delivered, their results are similar to those obtained in cases B2 and B3, with around 78-81% of those obtained in the 2-tank system. All this is possible with the use of a relatively small amount of encapsulated PCM, being most of the tank filled with the cheaper solid material.

Figures 8 and 9 show the temperature maps after reaching the periodic state, where the thermal buffering effect of the PCMs collocated at both ends of the tank can be observed. In each process, phase changing capsules located close to the fluid outlet, force the temperature of the outgoing HTF to remain close to the PCM melting point, and thus, inside the corresponding admissible range. This allows a longer operating time and a higher thermal filling of the whole tank.

Regarding the pressure losses produced by the presence of the filler material, it can be seen that they are negligible (less than 1% of total pressure losses). Pumping energy needed to overcome these, plus the gravitational force, represent less than 0.1% of the stored energy for all cases.

In summary, compared against solid-filled thermocline design, MLSPCM concept present higher storage capacity together with a higher efficiency in its utilization. Furthermore, although presenting lower overall capacity, MLSPCM prototypes yield a much higher efficiency than single-PCM ones, resulting in similar values of total energy storage.

3.1.2. Prototypes with larger diameter (13m $\times$ 43.7m)

Prototype C2 is probably the most cost-effective among those including encapsulated PCMs, due to its high efficiency and low amount of PCM used. However, in order to yield the same values of

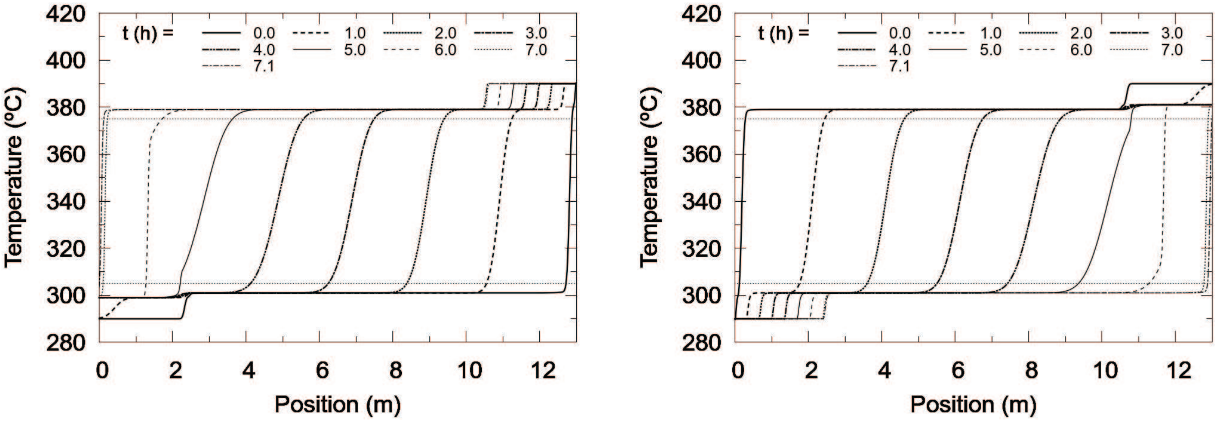

(a) Charge **(b)** Discharge

Figure 8: Case C1. Periodic state. Temperature maps at various instants. The chronological order of the curves is from right to left for the charge process and from left to right for the discharge. Horizontal dotted lines indicate the threshold temperatures.

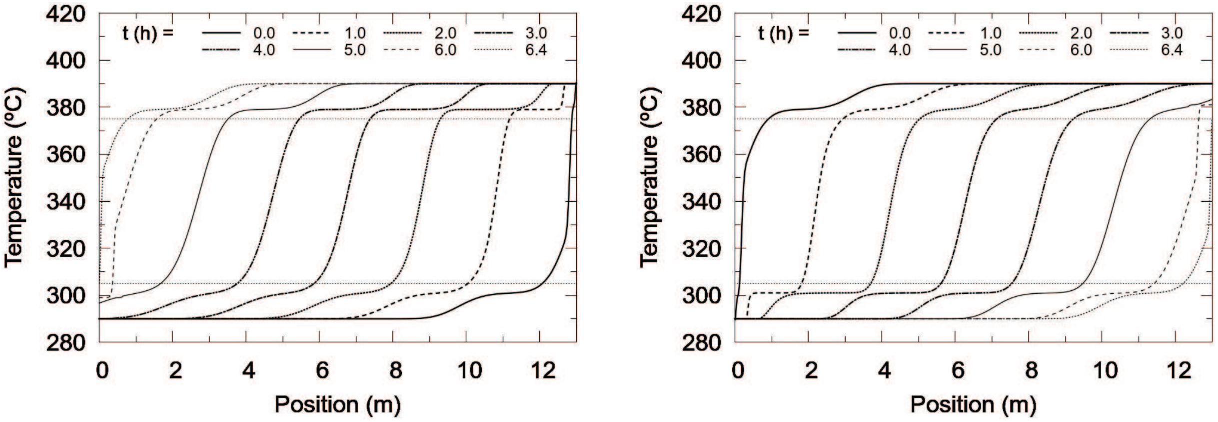

(a) Charge **(b)** Discharge

Figure 9: Case C2. Periodic state. Temperature maps at various instants. The chronological order of the curves is from right to left for the charge process and from left to right for the discharge. Horizontal dotted lines indicate the threshold temperatures.

energy —and more precisely, exergy — delivered to the power block as those of the 2-tank molten-salt system, the storage capacity of the single-tank system has to be increased. Hence, the tank diameter is enlarged.

Case C3 corresponds to this new case, with a tank diameter of 43.7m, where thermal performance values can be seen to be very similar to those of the ideal 2-tank system. The stored/released energy and exergy delivered to the PB are around 3% higher than with the 2-tank, while the efficiencies in the use of the total and latent capacities are very high.

This prototype has a volume 32% higher than one tank of the 2-tank system and requires around

68% less amount of molten salt than the latter. On the other hand, it needs to hold around 62% more weight and requires two small layers of encapsulated PCM (with less than 4% of total weight).

Case A2, which has the same tank dimensions as C3 but is totally filled with solid material, results in an effective storage of around 84% with respect to that of the 2-tank system and around 82% with respect to the obtained with C3.

Figures 10 and 11 depict the temperature maps of these two cases in the periodic state. It can be observed how the inclusion of the PCM layers induce a higher utilization of the sensible energy capacity of the tank, as already observed between cases A1 and C2.

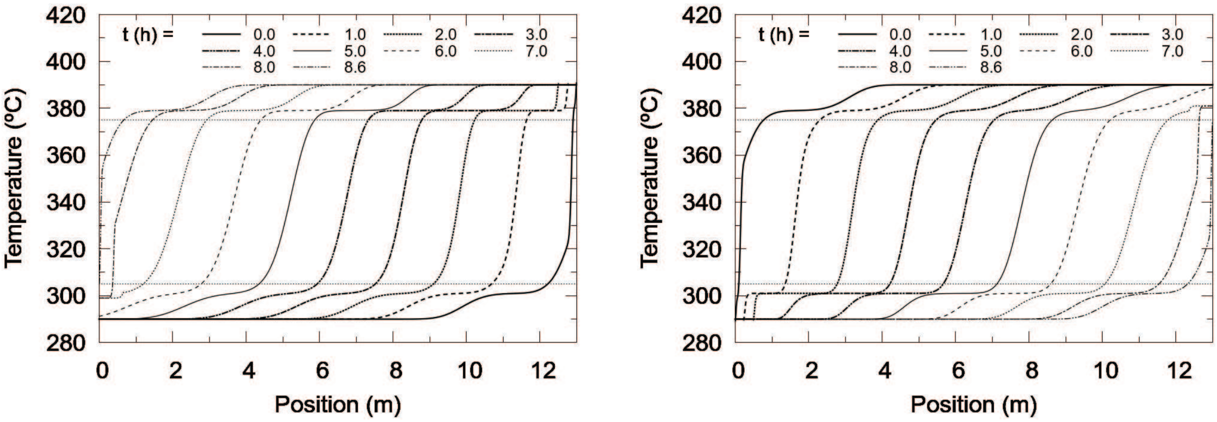

(a) Charge **(b)** Discharge

Figure 10: Case C3. Periodic state. Temperature maps at various instants. The chronological order of the curves is from right to left for the charge process and from left to right for the discharge. Horizontal dotted lines indicate the threshold temperatures.

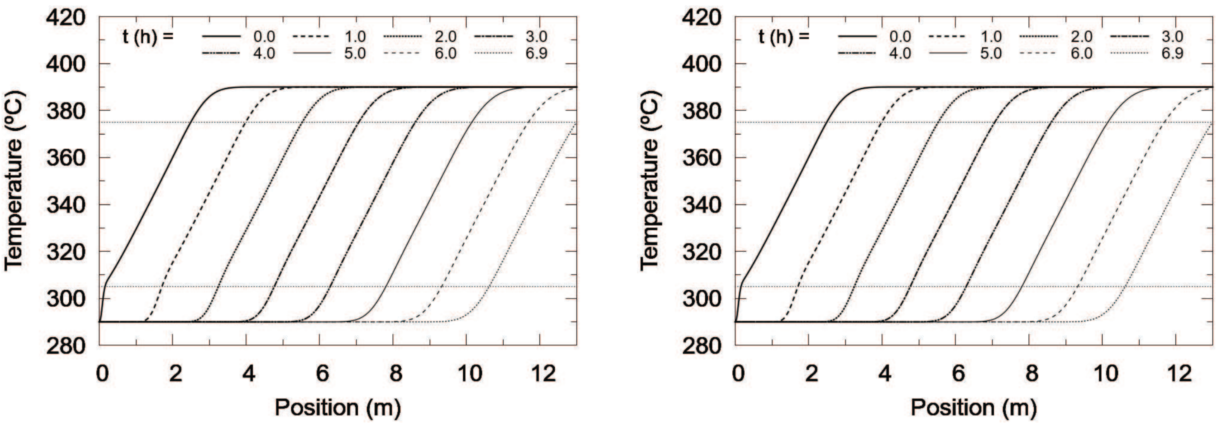

(a) Charge **(b)** Discharge

Figure 11: Case A2. Periodic state. Temperature maps at various instants. The chronological order of the curves is from right to left for the charge process and from left to right for the discharge. Horizontal dotted lines indicate the threshold temperatures.

In summary, a single-tank TES system equivalent to the reference 2-tank system, results smaller and more efficient when using an appropriate MLSPCM configuration than when using a solid-filler material.

4. Cases of TES integrated into a CSP facility

In this section, the analysis of the TES systems integrated into a CSP facility is performed, by taking into consideration the variations of the direct normal irradiation (DNI) on the solar field (SF), as well as the thermal energy losses to the ambient through the tank shell and foundation. Furthermore, idle processes are simulated; i.e. when there is no fluid flow through the tank.

The parameters for the reference CSP plant are shown in Table 5. The heat transfer fluid passing through the TES is molten salt. A sketch of the plant with a single-tank TES is shown in Fig. 12. The thermo-physical properties of the different materials in the packed beds are the same used for the previous cases. The efficiency of the heat exchanger intended to transfer heat between the fluids from the SF and TES is assumed to be 1.

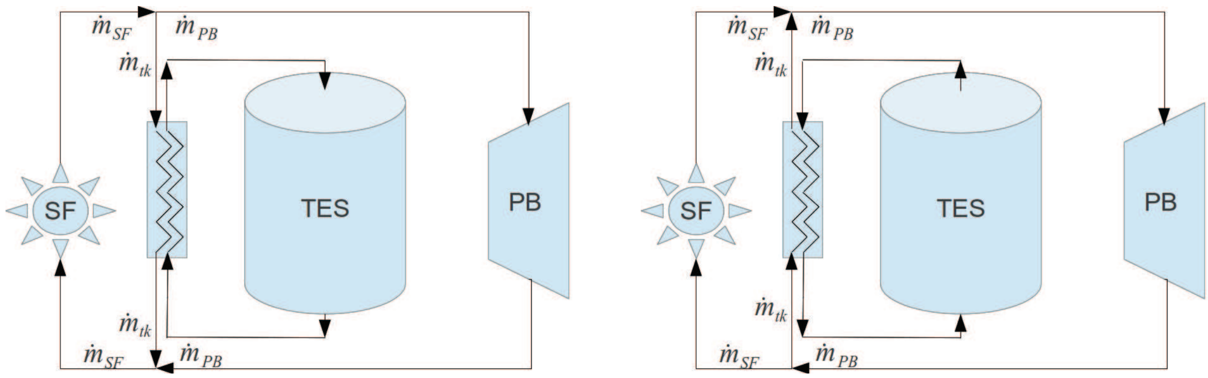

(a) Charge **(b)** Discharge

Figure 12: Sketch of CSP plant with single-tank TES.

4.1. Operating conditions

The same values of temperature of fluid coming from the solar field and from the power block (PB) as those of section 3 are adopted here, 390°C and 290°C, respectively. Furthermore, the same admissible temperature ranges are here considered, i.e. 375-390°C for the discharge and 290-305°C for the charge. However, one difference between the criterion used here and the one used in section 3 is that the temperature limits are not applied to the fluid flows coming out of the TES directly. Instead, the controlled temperature is that of the fluid coming into both, the SF and the PB. Hence, if the TES is being charged and the PB is generating power simultaneously, the fluid entering the SF is a

Table 5: Parameters of reference CSP plant

Turbine nominal power (MWe)	50
Solar field technology	Parabolic trough
Solar field area (m^2)	510120
Solar field peak efficiency (%)	70
Power block peak efficiency (%)	38
Storage capacity w/ 2-tank system (MWhth)	1152

mixture of the fluid streams coming from the PB and from the TES heat exchanger (see the sketch in Fig. 12a), and therefore, its temperature is not that of the cold fluid coming out of the TES but a weighted average of the temperatures of both streams. Something similar occurs with the temperature of the flow going to the PB if the TES is discharged at the same time as the SF is collecting heat (see the sketch in Fig. 12b). Therefore, the current criterion is less restrictive, from the point of view of the TES, since the temperature of the fluid coming out of it could be outside the corresponding admissible range but the process would not be stopped, as long as the temperature of the fluid coming into the receiving equipment still remains inside this range.

To avoid several charge and discharge processes being started and stopped in small time intervals, different (more restrictive) thresholds have been defined for starting the processes; i.e. a discharge is not initiated if the temperature at the top of the tank is lower than 380℃, while a temperature at the bottom of the tank higher than 300℃ is required for charging the tank.

The initial conditions for the TES, in the first day of simulation, are uniform temperatures of 290℃ for the whole tank and 15℃ for the soil.

The simulations are carried out for 17 days in summer (from June 30 to July 17) in Seville, Spain. The direct normal irradiation (DNI) and the rest of weather data are obtained from METEONORM software version 4.0. Table 6 depicts some basic information for this location.

For determining the power coming from the solar field, the following equation is used:

$$\dot{Q}_{SF} = DNI \times A_{SF} \times \eta_{SF}$$

where the DNI is multiplied by the surface area (A_{SF}) and overall efficiency of the solar field (η_{SF}), which is taken as the peak efficiency of the solar field in Andasol 1 plant [28] (see Table 5). It is assumed that the mass flow coming from the solar field is directly sent to the power block until the nominal power is reached, then, the excess flow is used to charge the storage system. When the mass flow from the SF is not enough to reach the nominal electric power, the TES discharge starts and the mass flow passing through the heat exchanger, placed between the SF and TES, is calculated as the difference between the mass flow coming from the SF and that needed for generating nominal power in the PB. The discharge continues until the threshold temperature is reached ($T_{PB} < 375$ ℃). After this, an idle process takes place until there is excess energy available to charge again the storage system.

The nominal thermal power, from the point of view of the TES, is calculated as:

$$\dot{Q}_{PB,nom} = \frac{\text{Nominal power}}{\eta_{PB} \times 0.98} = 134.26 \text{ MW}$$

where 0.98 is the assumed efficiency of the heat exchanger of the PB (not shown in figure 12) and η_{PB} is the efficiency of the PB (see Table 5).

From this value, the nominal molten salt mass flow passing through the TES is calculated as:

$$\dot{m}_{HTF,nom} = \frac{\dot{Q}_{PB}}{C_{p,HTF} \times \Delta T_{HTF}} = 894.2 \text{ kg/s} \tag{6}$$

where ΔT has been taken as 100℃ (290-390℃). This value is a little lower than the one used in section 3 (948 kg/s), which corresponds to that of Andasol 1 plant according to [28]. Therefore, $\dot{m}_{HTF,nom}$ is the mass flow passing through the TES in the discharge, when there is no available energy from the SF.

Table 6: Location basic data

Location	Latitude (º)	Longitude (º)	July T_{max} (℃)	July T_{min} (℃)	July DNI (kWh/m^2 day)
Seville, Spain	37.37	5.97	39.6	16.2	7.58

In figure 13, the curves of thermal power coming from the SF, thermal power needed to generate the nominal (electric) power in the PB and the remaining thermal power available to be stored in the TES, are plotted for the time range of the simulations.

4.2. Tank configurations

The same configurations tested in the simplified case (Table 1) are here tested, with the addition of the tank shell, insulation and foundation.

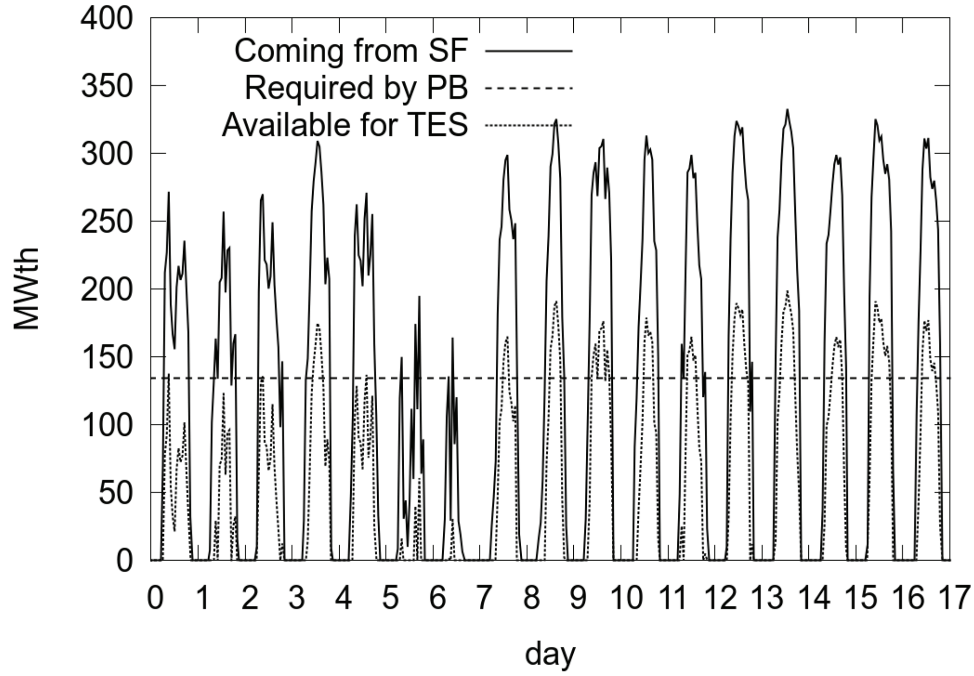

Figure 13: Thermal power (in MW) coming from the solar field, required by the power block (for nominal power generation) and available for storage, in the 17 days of simulation.

The tanks are made of steel A516gr70, while the insulation material for the lateral wall and roof is Spintex342G-100. The insulation is covered with a thin layer of aluminum 2024 T6.

Common geometric parameters for all the cases:

- Vertical wall thickness = 0.039 m.
- Bottom wall thickness = 0.021 m.
- Insulation thickness = 0.4 m.
- Foundation thicknesses: dry sand = 0.006 m; foam-glass = 0.420 m; heavy weight concrete = 0.450 m; soil = 9.140 m.

The thermo-physical properties of all the used materials can be found in [26].

4.3. Results and discussion

Table 7 shows the results for all the presented cases, which are expressed as mean values, per day, of the 17 days of simulation.

Firstly, it can be seen that the reference 2-tank TES shows zero energy losses, due to being considered as the ideal case, i.e. the hot tank is always at 390℃ and the cold tank at 290℃. However, the storage capacity is not entirely used because of the fact that not in some days there is not enough available energy (from the SF) to fill the 2-tank system completely. On the other hand, in some days there is an excess of energy and some has to be discarded (see the "unused available energy" row in Table 7), probably by defocusing some collector lines in the solar field.

In the last row of Table 7, the number of days for which the temperature threshold is reached by the outlet fluid in the charging process is presented. This can be seen as the number of days in which the effective thermal capacity is exhausted. The term "effective" is used in order to differentiate between the capacity indicated in Table 3, which is the ideal capacity and does not depend on the temperature thresholds, and the "real" one which is the one that results from the simulations with the restrictions in the outlet temperature. In the case of the 2-tank, since the threshold is never reached, the number of days in which the system is totally charged is indicated.

The fact of not exhausting the effective capacity in every day of simulation distinguishes the present operating conditions from those of section 3, since in the latter the charge was not stopped until the temperature threshold was reached.

The differences in the values of total energy coming from the SF and available energy for storage, between the different prototypes, is due to interpolation errors of the input data. These are available at intervals of one hour and are needed for each time step of simulation, with a frequency in the order of seconds and dynamically determined by the code, resulting in different interpolation steps for each case.

Table 7: Performance results for each configuration.

	Diameter = 38m							Diameter = 43.7m	
Results	2-tank	A1	B1	B2	B3	C1	C2	C3	A2
Total energy from SF (MWh)	2798.6	2776.3	2776.1	2776.1	2780.8	2776.3	2776.3	2776.6	2776.3
Energy available for charging the TES (MWh)	1151.0	1125.8	1126.2	1126.1	1126.2	1125.8	1125.8	1125.8	1125.8
Energy delivered to the PB by the TES (MWh)	959.4	715.3	397.0	794.6	762.4	805.7	777.3	963.6	879.0
Energy delivered by TES / TES capacity (%)	83.3	78.1	27.8	55.6	53.3	71.8	80.3	75.3	72.5
Energy delivered by TES / Delivered by 2-tank (%)	100.0	74.6	41.4	82.8	79.5	84.0	81.0	100.4	91.6
Energy losses (MWh)	0.0	3.4	3.6	3.3	3.4	3.4	3.4	4.2	4.3
Energy losses / Energy delivered to PB by TES (%)	0.0	0.4	0.9	0.4	0.4	0.4	0.4	0.4	0.5
Exergy delivered to the PB by the TES (MWh)	460.6	343.2	190.3	379.1	365.7	384.4	372.4	461.6	421.7
Exergy Delivered/ Delivered by 2-tank (%)	100.0	74.5	41.3	82.3	79.4	83.5	80.8	100.2	91.5
Unused available energy (MWh)	191.6	402.9	692.1	221.7	330.5	311.3	342.9	154.8	236.1
Nº of days in with the charge is stopped by threshold	10[1]	13	14	12	12	12	12	9	11

[a]Temperature thresholds are never reached by the 2-tank TES, and therefore, the number of days correspond to those when the system is totally charged.

For the solid-filled thermocline prototype A1, the values of energy and exergy delivered to the PB are lower than those obtained with the 2-tank (74.5%). However, these differences are not as high as those shown in section 3. This is in part due to the variability of the available energy for storage, which in some days is lower than the storage capacity, and also to the less restrictive operating conditions for the TES (mentioned above), which allow a greater thermal filling than that allowed in section 3. Figure 14 shows the initial and final temperature maps for charge and discharge processes in the 10$^{\text{th}}$ day, with durations of more than 6 hours each. It can be observed that the final temperature at the charge goes beyond the threshold (305°C) due to the mixing effect mentioned before, and that the tank is thermally filled to a higher extent than in section 3 (compare with Fig. 4). The difference between the temperature maps at the end of the charge and at the start of the discharge is because an idle process of around 5.5 hours and another charge of around 18 minutes occur between them. Comparing the number of days in which the storage tank "effective" capacity is exhausted, it is observed that this happens in 10 days for the 2-tank system and in 13 for A1. As mentioned above, this explains why the efficiency in the use of total capacity is closer between the 2-tank and A1 prototypes than in section 3, where all the prototypes were charged until reaching the threshold temperature.

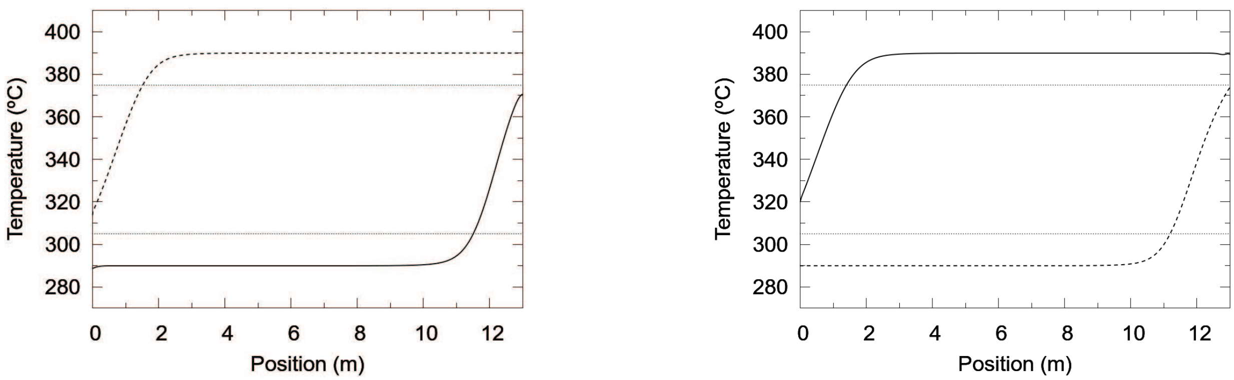

(a) Charge **(b)** Discharge

Figure 14: Temperature maps of day 10 for charge and discharge processes for prototype A1. Solid line indicates the temperature at the start of the process and dashed line at the end. Horizontal dotted lines indicate the threshold temperatures.

For prototype B1, the results are much worse, being in agreement with those obtained previously. Similarly as in section 3, the results for prototypes B2 and B3 are much better than for B1 and comparable to those of C2, in terms of total energy and exergy delivered, but worse than the latter in terms of efficiency.

MLSPCM prototypes C1 and C2 result in a storage of around 84% and 80% compared to the 2-tank, respectively. Their efficiency in the use of total capacity is lower than that obtained in section

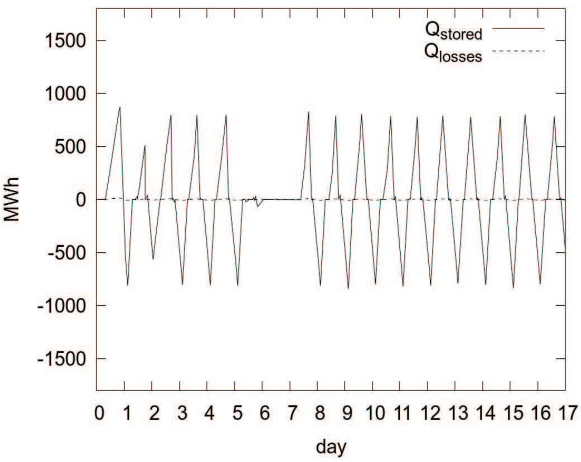

(a) A1

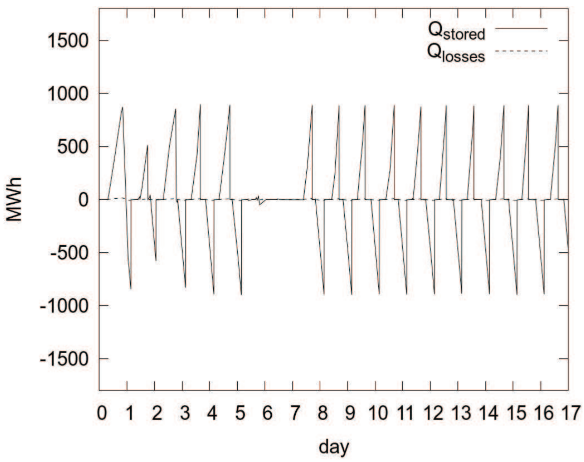

(b) C2

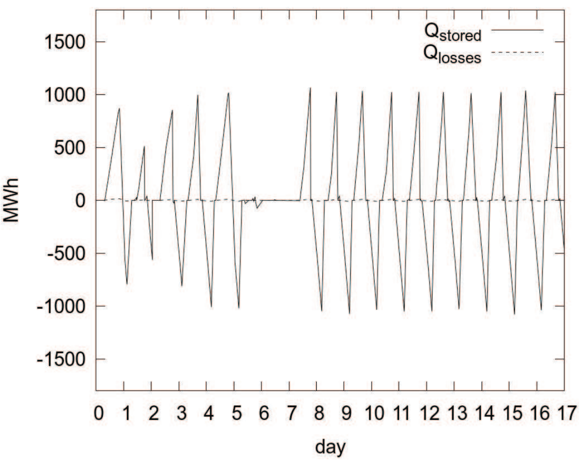

(c) A2

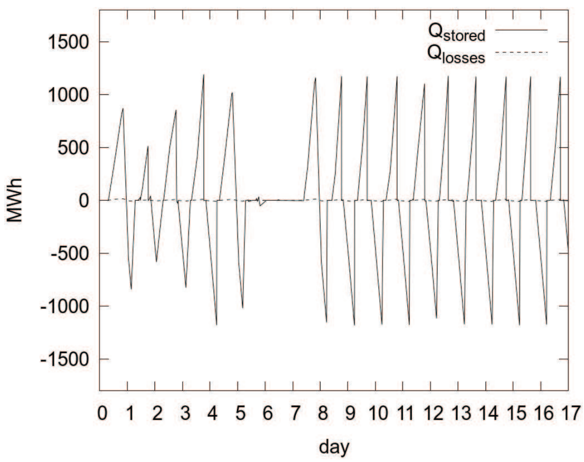

(d) C3

Figure 15: Evolution of the energy stored and lost for several prototypes. Values are reset to 0 at the end of each process. Stored energy (continuous line) has positive values in the charge and negative values in the discharge. Thermal losses (dashed line) are positive when heat comes out of the packed bed (by conduction through the walls) and negative when it comes into it.

3, which again, is mostly due to the occurrence of days of low radiation in which the available energy is not enough to fill the TES. The total energy effectively stored is closer to that obtained by prototype A1, although still higher. C2 still results in a higher use of the storage capacity than A1, but C1 shows a lower value.

Prototype C3, which has the same configuration as C2 but with a higher diameter, is seen to result in almost the same amount of exergy delivered to the power block as in the 2-tank system, and therefore it is considered as equivalent to the latter, since it would result in almost the same amount of power generation. When comparing energy efficiencies of prototypes C3 and A2 it can be observed that it is higher in the former than in the latter (75.3% vs 72.5%), but similar. Case A2 delivers

91.5% of the exergy delivered by the ideal 2-tank. This is 9% lower than that achieved by the C3 configuration, which makes use of the latent heat capacity of the PCM layers.

In Fig. 15, the energy stored and lost for prototypes A1, C2, A2 and C3 are plotted for each day. It can be seen that in the first days there is a significant variation of stored/delivered energy and from the 8$^{\text{th}}$ day on, it is stabilized. This is due, on the one hand, to the particular initial conditions of the first day (uniform low temperature), and on the other, to the DNI variations in the first seven days. Particularly, in days 6 and 7 all the TES remain uncharged due to the low amount of available irradiation.

In all cases, the thermal losses are very low (less than 1% of the energy delivered to the PB by the TES for all the cases, and around 0.5% for most), which is an indication of having enough thermal insulation. Due to the transient operation of the tanks, in the discharge processes heat comes into to the packed bed through the tank walls and foundation instead of coming out, and therefore, these components act as additional thermal storage media.

5. Conclusions

MLSPCM thermocline-like thermal energy storage prototypes have been designed for their utilization in a CSP plant. A parabolic trough plant of 50MWe, similar to Andasol 1 (Granada, Spain), has been adopted as reference. The analysis has been carried out using verified and validated models of the thermocline-like configurations, tank walls and foundation.

Two different analyses were performed, one centered in evaluating the performance of the TES systems under specific conditions, in which the TES is charged and discharged consecutively until reaching a periodic steady state; and another in which the same TES configurations are tested under 17 days of operation in the reference CSP plant. In the latter case, weather conditions of Seville (Spain) were adopted, the variation of the operating conditions due to the changes in the direct normal irradiation were simulated, and the tank walls and foundation were taken into account.

MLSPCM single-tank systems, with the same tank dimensions as one of the two-tank molten salt tanks, were compared to the latter system as well as to other single-tank configurations. Furthermore, one of the MLSPCM configurations was chosen for designing a bigger tank, aimed to achieve the same amount of energy stored as that of the two-tank system.

The first analysis confirms the conclusions taken in previous works [18, 19], indicating that MLSPCM configurations diminish the degradation of the thermocline of single-tank solid-filled designs, produced by the restrictions in the outflow temperature. Hence, both total capacity and the extent at which it is harnessed are increased. Compared against single-PCM packed beds, MLSPCM designs yield a much higher efficiency in the use of total capacity, especially when the amount of PCM effectively changing phase is evaluated. Compared against the two-tank system, MLSPCM prototype C3 is considered as its equivalent in terms of energy and exergy delivered to the power block, with a volume 32% higher than that of one of the two tanks and needing only 32% of the amount of molten-salt. On the other hand, the total weight hold by C3 is 62% higher and it needs a relatively small amount of PCM (less than 4% of total weight). If the comparison is performed against a single-solid filled thermocline tank with the same dimensions (i.e. prototype A2), C3 stores around 20% more energy/exergy, holding almost the same weight (around 3% less) and needing around 8% more molten-salt, besides the extra PCM layers.

The second analysis, incorporating more aspects related to the operation of the CSP plant, result in lower differences between the performance of MLSPCM and single-solid thermocline configurations. On one hand, the restrictions on the temperature of the heat transfer fluid are not applied to the flow coming out of the TES, but to that entering the solar field or the power block. This change results in less restrictive operating conditions for the TES, and therefore, the thermocline degradation occurring in the single-solid filled thermocline is not so high. Furthermore, the fact of having days of low radiation result in a penalization of the capacity factor of the systems with higher capacity. Nevertheless, in this analysis, the MLSPCM prototypes tested still show higher values of stored energy/exergy and efficiency (C2 and C3) than single-solid thermocline tanks. When compared against the reference 2-tank system, prototype C3 is still considered equivalent to it, since the values of stored energy and exergy are almost exactly the same. In these conditions, prototype A2 delivers around 10% less energy/exergy to the power block than C3 in the 17 days of simulation.

Thermal losses to the ambient are observed to be very low for all the cases (less than 1%), and the tank walls and foundation act as extra thermal storage media.

As in previous works, MLSPCM concept shows to be a promising alternative to the other TES configurations tested —due to the combination of higher storage capacity and higher efficiency in its use— as well as to the standard two-tank system.

However, variability of operating conditions are seen to affect the relative advantage of using one or another TES system, and therefore, it is possible that TES designs which are optimal for the isolated conditions are not so for the real application. Optimization of MLSPCM designs to one or another CSP facility needs to be studied in further detail, with long-term simulations incorporating all the relevant aspects, such as the real limitations for the HTF temperature, the different thermo-physical properties of the available PCMs and an economic evaluation.

Acknowledgments

This work has been financially supported by the *Ministerio de Economía y Competitividad, Secretaría de Estado de Investigación, Desarrollo e Innovación*, Spain (ENE-2011-28699), by the EIT via the KIC InnoEnergy TESCONSOL project (ref. 20_2011_IP16) and by the *Secretaria d'Universitats i Recerca (SUR) del Departament d'Economia i Coneixement (ECO) de la Generalitat de Catalunya* and by the European Social Fund.

References

[1] M. Medrano, A. Gil, I. Martorell, X. Potau, and L. F. Cabeza, "State of the art on high temperature thermal ebergy storage for power generation. part 2—Case studies," *Renew. Sust. Energ. Rev.*, no. 14, pp. 56–72, 2010.

[2] G. J. Kolb, C. K. Ho, T. R. Mancini, and J. A. Gary, "Power tower technology roadmap and cost reduction plan," Tech. Rep. SAND2011-2419, Sandia National Laboratories, 2011.

[3] U. Herrmann, B. Kelly, and H. Price, "Two-tank molten salt storage for parabolic trough solar power plants," *Energy*, vol. 29, pp. 883–893, 2004.

[4] J. I. Ortega, J. I. Burgaleta, and F. M. Téllez, "Central receiver system solar power plant using molten salt as heat transfer fluid," *J. Sol. Energ.-T. ASME*, vol. 130, pp. 024501–1–6, 2008.

[5] J. E. Pacheco, S. K. Showalter, and W. J. Kolb, "Development of a molten-salt thermocline thermal storage system for parabolic trough plants," *J. Sol. Energ.-T. ASME*, vol. 124, pp. 153–159, 2002.

[6] A. Yang and S. V. Garimella, "Molten-salt thermal energy storage in thermoclines under different environmental boundary conditions," *Appl. Energ.*, vol. 87, pp. 3322–3329, 2010.

[7] R. Tamme, D. Laing, and W. D. Steinmann, "Advanced thermal energy storage technology for parabolic trough," *J. Sol. Energ.-T. ASME*, vol. 126, pp. 794–800, 2004.

[8] J. L. Shyu, R.J. and L. Fang, "Thermal analysis of stratified storage tanks," *J. Sol. Energ.-T. ASME*, vol. 111, pp. 54–61, 1989.

[9] I. Rodríguez, J. Castro, C. Pérez-Segarra, and A. Oliva, "Unsteady numerical simulation of the cooling process of vertical storage tanks under laminar natural convection," *Int. J. Therm. Sci.*, vol. 48, pp. 708–721, 2009.

[10] L. J. Shah and S. Furbo, “Entrance effects in solar storage tanks,” *Sol. Energy*, vol. 75, pp. 337–348, 2003.

[11] N. Calvet, J. C. Gomez, A. Faik, V. V. Roddatis, A. Meffre, G. C. Glatzmaier, S. Doppiu, and X. Py, “Compatibility of a post-industrial ceramic with nitrate molten salts for use as filler material in a thermocline storage system,” *Appl. Energ.*, vol. 109, pp. 387–393, 2013.

[12] H. Michels and R. Pitz-Paal, “Cascaded latent heat storage for parabolic trough solar power plants,” *Sol. Energy*, vol. 81, pp. 829–837, 2007.

[13] M. Liu, W. Saman, and F. Bruno, “Review on storage materials and thermal performance enhancement techniques for high temperature phase change thermal storage systems,” *Renew. Sust. Energ. Rev.*, vol. 16, pp. 2118–2132, 2012.

[14] H. Shabgard, C. W. Robak, T. L. Bergman, and A. Faghri, “Heat transfer and exergy analysis of cascaded latent heat storage with gravity-assisted heat pipes for concentrating solar power applications,” *Sol. Energy*, vol. 86, no. 3, pp. 816–830, 2012.

[15] K. Nithyanandam, R. Pitchumani, and A. Mathur, “Analysis of a latent thermocline storage system with encapsulated phase change materials for concentrating solar power,” *Appl. Energ.*, vol. 113, pp. 1446–1460, 2014.

[16] S. M. Flueckiger and S. V. Garimella, “Latent heat augmentation of thermocline energy storage for concentrating solar power —A system-level assessment,” *Appl. Energ.*, vol. 116, pp. 278–287, 2014.

[17] W. Steinmann and R. Tamme, “Latent heat storage for solar steam systems,” *J. Sol. Energ.-T. ASME*, vol. 130, pp. 011004–1–011004–5, 2008.

[18] P. Galione, C. D. Pérez-Segarra, I. Rodríguez, A. Oliva, and J. Rigola, “Multi-layered solid-PCM thermocline thermal storage concept for CSP plants. Numerical analysis and perspectives,” *Appl. Energ.*, vol. 142, pp. 337–351, 2015.

[19] P. Galione, C. D. Pérez-Segarra, I. Rodríguez, O. Lehmkuhl, and J. Rigola, “A new thermocline-pcm thermal storage concept for CSP plants. Numerical analysis and perspectives,” in *Proceedings of the SolarPACES 2013 International Conference*, vol. 49 of *Energy Procedia*, pp. 790–799, Elsevier, 2014.

[20] R. Damle, O. Lehmkuhl, G. Colomer, and I. Rodríguez, “Energy simulation of buildings with a modular object-oriented tool,” in *Proc. ISES Solar World Congress 2011*, 2011.

[21] N. Wakao, S. Kaguei, and T. Funazkri, “Effect of fluid dispersion coefficients on particle-to-fluid heat transfer coefficients in packed beds,” *Chem. Eng. Sci.*, vol. 34, pp. 325–336, 1979.

[22] R. Krupiczka, “Analysis of thermal conductivity in granular materials,” *Int. Chem. Eng.*, vol. 7, no. 1, pp. 122–144, 1967.

[23] A. Nakayama, F. Kuwahara, and Y. Kodama, “An equation for thermal dispersion flux transport and its mathematical modelling for heat and fluid flow in a porous medium,” *J. Fluid Mech*, vol. 563, pp. 81–96, 2006.

[24] R. G. Holdich, *Fundamentals of particle technology.* Midland Information Technology and Publishing, 2002.

[25] N. Nallusamy, S. Sampath, and R. Velraj, “Experimental investigation on a combined sensible and latent heat storage system integrated with constant/varying (solar) heat sources,” *Renew. Energ.*, vol. 32, pp. 1206–1227, 2007.

[26] I. Rodríguez, C. D. Pérez-Segarra, O. Lehmkuhl, and A. Oliva, “Modular object-oriented methodology for the resolution of molten salt storage tanks for CSP plants,” *Appl. Energ.*, vol. 109, pp. 402–414, 2013.

[27] S. Torras, C. D. Pérez-Segarra, I. Rodríguez, J. Rigola, and A. Oliva, “Parametric study of two-tank TES systems for CSP plants,” in *Proceedings of the SolarPACES 2014 International Conference*, 2014.

[28] U. Herrmann and R. Kistner, “The Andasol Project,” tech. rep., FLABEG Solar Int. GmbH, Solar Millennium AG, 2002. Workshop on Thermal Storage for Trough Power Systems, `http://www.nrel.gov/csp/troughnet/pdfs/uh_anda_sol_ws030320.pdf`.

[29] A. B. Zavoico, “Solar power tower design basis document,” Tech. Rep. SAND2001-2100, Sandia National Laboratories, 2001.

[30] C. Xu, Z. Wang, Y. He, X. Li, and F. Bai, “Sensitivity analysis of the numerical study on the thermal performance of a packed-bed molten salt thermocline thermal storage system,” *Appl. Energ.*, vol. 92, pp. 65–75, 2012.